

Estimating Earthquake Source Parameters from Geodetic Measurements

Kurt L. Feigl

Centre National de la Recherche Scientifique, Toulouse, France

1. Brief Summary of Applicable Techniques

Figure 1 sketches the geometry of the various geodetic techniques for coseismic surveying. I will emphasize the new INSAR technique because the older techniques have been described well elsewhere and the newer SLR, VLBI, and DORIS techniques apply only to a few earthquakes.

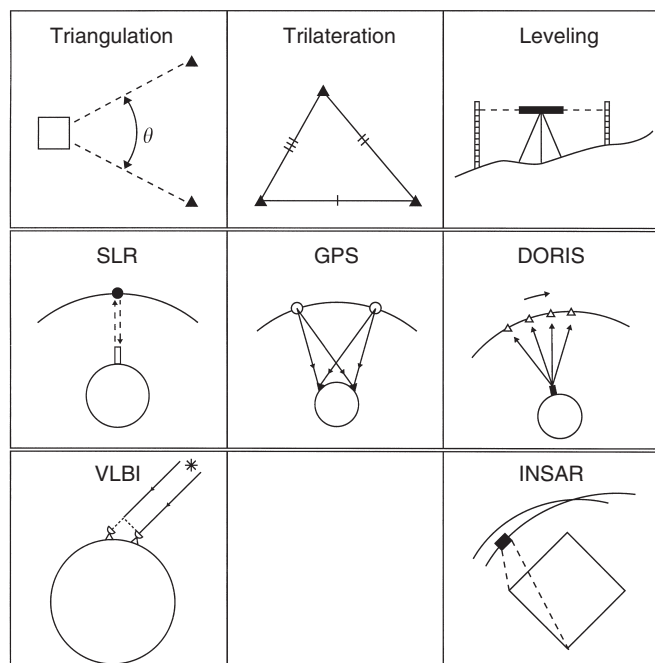


FIGURE 1. Sketch of geometry for various geodetic techniques.

1.1 Ground-based Vertical Techniques

Spirit leveling measures the difference in elevation between pairs of points. Errors accumulate with the square root of the length L of the “line” (almost always a road) between the points. Typical first-order leveling measurements have a standard deviation of the order of $L^{1/2}$ mm with L in km, i.e., ~ 10 mm over 100 km (Bomford, 1980). Bilham (1991) reviews geophysical applications of this technique.

Leveling measures heights with respect to the geoid (or “mean sea level”). Such “orthometric” heights are not to be confused with the “ellipsoidal” heights provided by some GPS instruments. The difference between the two is typically of the order of 10 m, and represents the undulation of the geoid. In the excitement immediately following an earthquake, scientists often consider remeasuring an old leveling line with GPS. Although this approach will not measure coseismic displacements, it can detect a different quantity — the geoid (Milbert and Dewhurst, 1992; Calais *et al.*, 1993).

Leveling is the ground-based technique of choice for measuring vertical coseismic displacements larger than about a centimeter. It seems to work best for normal-faulting events with magnitude of 6 or larger where surface rupture creates a spectacular offset, for example, the 1983 Borah Peak earthquake (Stein and Barrientos, 1985; Ward and Barrientos, 1986). Leveling data can also provide useful information in thrusting events without surface rupture, such as the 1989 Loma Prieta earthquake (see references in Table 1).

Sea level as recorded by tide gauges can also reveal vertical coseismic motion, as in the great 1964 Alaska earthquake (Holdahl and Sauber, 1994) (see Bilham (1991) for a review). If the coseismic motion is upwards on a coastline, it will kill mollusks by removing them from the water. Their new position above sea level records the vertical displacement with

TABLE 1 Earthquake Parameters Estimated from Space-based Geodesy and Seismology

Year	Month	Day	Name	M_w or M_s	Seismic Moment (10^{18} Nm)	Geodetic Moment (10^{18} Nm)	Data ^a	Reference
1906	4	18	San Francisco, California	7.7	470.00	750.00	TR	Thatcher <i>et al.</i> (1997)
1906	4	18	San Francisco, California	7.7	470.00	555.00	TR	Matthews and Segall (1993)
1923	9	1	Kanto, Japan	8.2	573.30	1603.27	LL	Kanamori (1973)
1934	6	8	Parkfield, California	6.0		4.40	TR	Segall and Du (1993)
1944	12	7	Tonanki, Japan	8.1	1500.00	2000.00	TR, tsunami	Satake (1993)
1946	12	20	Nankaido, Japan	8.1	1500.00	3900.00	TR, tsunami	Satake (1993)
1954	9	9	El Asnam, Algeria	6.7		9.80	LL	Bezzeghoud <i>et al.</i> (1995)
1959	8	18	Hebgen Lake, Montana	7.3	103.00	120.00		Barrientos <i>et al.</i> (1987)
1960	5	22	Chile	9.5	2 000 000.00	94 000.00	SL, TG, TR	Barrientos and Ward (1990)
1964	3	28	Alaska	9.2	75 000.00	50 000.00	LL, TR, TG	Holdahl and Sauber (1994)
1966	6	28	Parkfield, California	6.0	1.40	4.40	TR, TL	Segall and Du (1993)
1971	2	9	San Fernando, California	6.4			LL, TR, TG	Meade and Miller (1973); Morrison (1973)
1976	7	28	Tangshan, China	7.8	120.00	98.00	LL	Huang and Yeh (1997)
1976	7	28	Luanxian, China	7.8	0.00	19.00	LL	Huang and Yeh (1997)
1976	11	15	Ningho, China	7.8	0.00	8.90	LL	Huang and Yeh (1997)
1978	6	20	Thessalanoki, Greece	6.4	2.70	4.00	LL	Stiros and Drakos (2000)
1978	11		Asal, Djibouti	5.3	0.17	0.60	TR, LL	Lépine <i>et al.</i> (1979); Ruegg <i>et al.</i> (1979); Stein <i>et al.</i> (1991)
1979	3	15	Homestead Valley, California	5.9	0.36	0.44	TR	Savage <i>et al.</i> (1993)
1979	10	15	Imperial Valley, California	6.5				Crook <i>et al.</i> (1982); Harsh (1982)
1980	10	10	El Asnam, Algeria	7.3	50.00	62.00	TR, LL	Ruegg <i>et al.</i> (1982)
1983	5	2	Coalinga, California	6.5			LL	Hartzell and Heaton (1983); Stein and King (1984); Eberhardt-Phillips (1989)
1983	10	28	Borah Peak, Idaho	7.3	18.50	25.00	LL	Stein and Barrientos (1985)
1985	8	4	Kettleman Hills, California	6.1	1.60	1.25	LL	Ekstrom <i>et al.</i> (1992)
1986	7	8	North Palm Springs, California	6.0	0.97	0.69	TL	Savage <i>et al.</i> (1993)
1987	11	17	Gulf of Alaska	6.9	0.00	66.00	VLBI	Sauber <i>et al.</i> (1993)
1987	11	24	Superstition Hills, California	6.2	9.00	9.40	TL	Larsen <i>et al.</i> (1992)
1988	3	6	Gulf of Alaska	7.6	1115.00	1220.00	VLBI	Sauber <i>et al.</i> (1993)
1989	6	26	Kiluaea South Flank, Hawaii	6.1	5.20	8.00	LL	Arnadottir <i>et al.</i> (1991)
1989	6	26	Kalapana, Hawaii	6.1	5.20	8.00	LL	Arnadottir <i>et al.</i> (1991)
1989	6	26	Kalapana, Hawaii	6.1	5.20	10.00	GPS	Dvorak (1994)
1989	10	1	Whittier Narrows, California	5.9	0.10	0.10	LL	Lin and Stein (1989)
1989	10	18	Loma Prieta, California	7.1	23.00	29.00	LL	Marshall <i>et al.</i> (1991)
1989	10	18	Loma Prieta, California	7.1	23.00	30.00	TL&GPS	Lisowski <i>et al.</i> (1990)
1989	10	18	Loma Prieta, California	7.1	23.00	34.00	TL, GPS, LL	Arnadottir and Segall (1994)
1989	10	18	Loma Prieta, California	7.1	23.00	27.00	TL, GPS, LL	Arnadottir and Segall (1994)
1989	10	18	Loma Prieta, California	7.1	23.00	29.00	TL, GPS, LL	Arnadottir and Segall (1994)
1989	10	18	Loma Prieta, California	7.1	23.00	29.00	GPS	Williams <i>et al.</i> (1993)
1991	4	22	Valle de la Estrella, Costa Rica	7.7			GPS	Lundgren <i>et al.</i> (1993)
1992	4	23	Joshua Tree, California	7.1	2.00	1.84	TL	Savage <i>et al.</i> (1993)
1992	4	23	Joshua Tree, California	6.1	2.15	1.70	TL, GPS	Bennett <i>et al.</i> (1994)
1992	4	25	Cape Mendocino, California	7.1	44.50	31.00	LL, TL, GPS	Murray <i>et al.</i> (1996)
1992	6	28	Big Bear, California	6.3	5.20	4.20	GPS	Murray <i>et al.</i> (1993)
1992	6	28	Big Bear, California	6.3	5.20	3.70	GPS	Johnson <i>et al.</i> (1994)
1992	6	28	Landers, California	7.3	80.00	79.00	GPS	Murray <i>et al.</i> (1993)
1992	6	28	Landers, California	7.3	80.00	80.00	CGPS	Bock <i>et al.</i> (1993)
1992	6	28	Landers, California	7.3	80.00	103.00	GPS	Hudnut <i>et al.</i> (1994)
1992	6	28	Landers, California	7.3	80.00	77.00	Joint	Wald and Heaton (1994)
1992	6	28	Landers, California	7.3	80.00	99.50	GPS	Johnson <i>et al.</i> (1994)
1992	6	28	Landers, California	7.3	80.00	90.00	GPS	Freymueller <i>et al.</i> (1994)
1992	12	2	Fawnskin, California	5.1	0.04	0.00	INSAR	Feigl <i>et al.</i> (1995)
1993	5	17	Eureka Valley, California	6.1	1.20	1.70	INSAR	Massonnet and Feigl (1995b)
1993	5	17	Eureka Valley, California	6.1	1.20	0.00	INSAR	Peltzer and Rosen (1995)
1993	8	8	Guam	7.8			GPS	Beavan <i>et al.</i> (1994)
1994			Kamchatka				DORIS	A. Cazenave, personal commun. (1999);
1994			Sanriku-Haruka-Oki, Japan	7.5				Miyazaki <i>et al.</i> (1996)

(continued)

TABLE 1 (continued)

Year	Month	Day	Name	M_w or M_s	Seismic Moment (10^{18} Nm)	Geodetic Moment (10^{18} Nm)	Data ^a	Reference
1994	1	17	Northridge, California	6.7	11.00	13.00	Joint	Wald <i>et al.</i> (1996)
1994	1	17	Northridge, California	6.7	11.00	10.07	INSAR	Massonnet <i>et al.</i> (1996a)
1994	1	17	Northridge, California	6.7	11.00	15.80	TERRAscope	Thio and Kanamori (1996)
1994	1	17	Northridge, California	6.7	11.00	13.40	GPS	Shen <i>et al.</i> (1996) model A
1994	1	17	Northridge, California	6.7	11.00	16.30	GPS	Hudnut <i>et al.</i> (1995)
1994	1	17	Northridge, California	6.7	11.00		INSAR	Murakami <i>et al.</i> (1996)
1994	2	15	Liwa	6.8			GPS	Duquesnoy <i>et al.</i> (1996)
1994	6	18	Arthur's Pass, New Zealand	6.7	13.00	16.00	GPS	Arnadottir <i>et al.</i> (1995)
1994	10	4	Hokkaido-Toho-Oki, Japan	8.1	0.00	2000.00	GPS	Tsuji <i>et al.</i> (1995)
1995			Hyogo-ken Nanbu (Kobe), Japan	7.2			GPS	Tabei <i>et al.</i> (1996)
1995			Hyogo-ken Nanbu (Kobe), Japan	7.2			INSAR	Ozawa <i>et al.</i> (1997)
1995	5	13	Grevena, Greece	6.6	7.60	16.30	GPS	Clarke <i>et al.</i> (1996); Clarke <i>et al.</i> (1998)
1995	5	13	Grevena, Greece	6.6	7.60	6.40	INSAR	Meyer <i>et al.</i> (1996); Meyer <i>et al.</i> (1998)
1995	6	15	Corinth, Greece	6.2	4.00	3.90	Joint	Bernard <i>et al.</i> (1997)
1995	7	30	Antofogasta, Chile	8.1	1700.00	1500.00	GPS, SL	Ruegg <i>et al.</i> (1996)
1995	7	30	Antofogasta, Chile	8.1	1700.00	1420.00	GPS, SW	Ihmlé and Ruegg (1997)
1995	7	30	Antofogasta, Chile	8.1	1700.00	1780.00	GPS	Klotz <i>et al.</i> (1999)
1995	10	1	Dinar, Turkey	6.1	3.10	3.18	INSAR	Wright <i>et al.</i> (1999)
1995	10	9	Jalisco, Mexico	8.0			INSAR	Vincent (1998)
1995	10	9	Jalisco, Mexico	8.0			GPS	Melbourne <i>et al.</i> (1997)
1996	2	26	St. Paul de Fenouillet, France	5.0		0.04	INSAR	Rigo and Massonnet (1999)
1999	8	24	Izmit, Turkey	7.4	195.00	170.00	GPS	Reilinger <i>et al.</i> (2000)
1999	10	16	Hector Mines, California	7.1			INSAR	Sandwell <i>et al.</i> (2000)

^aLL = Leveling, TR = Triangulation, TL = Trilateration, TG = Tide gauge, SL = Sea level from mollusks, and SW = Surface waves.

a precision of the order of a decimeter, as in two Chilean earthquakes (Barrientos and Ward, 1990; Ruegg *et al.*, 1996). This “natural tide gauge” is the only way other than mapping surface rupture to measure coseismic displacements without planning an observation before the earthquake.

1.2 Triangulation and Trilateration Surveying

Triangulation measures the angle between two benchmarks as seen from a third with a precision of $4 \mu\text{rad}$ at best (Bomford, 1980). Now classic, this technique nonetheless established the relative positions of the vast majority of benchmarks in most national geodetic networks. For many earthquakes, these measurements are the only ones acquired before the earthquake, for example the great 1906 San Francisco earthquake (Thatcher, 1974; Matthews and Segall, 1993; Thatcher *et al.*, 1997) and other studies in California (Savage and Burford, 1970).

Trilateration measures the distance between two benchmarks with a precision of the order of a centimeter (Bomford, 1980). For earthquake studies, its use seems to be limited mostly to California (Prescott *et al.*, 1979), although an early study in the Afar revealed over 2 m of displacement (Ruegg *et al.*, 1979).

Both triangulation and trilateration require a clear line of sight between the benchmarks, limiting their use to distances typically less than 30 or 50 km at most. As a result, many benchmarks were installed on hilltops and mountain tops with difficult access, the most extreme examples being the peaks in the High Karakoram (Chen *et al.*, 1984) and even the summit of Mt. Everest (Bilham, 1998). This offers the advantage of conserving the benchmark from destruction for long periods of time. Interestingly, many of these older benchmarks on summits continue to serve because they also provide an unobstructed line of “sight” to orbiting satellites. Also, these rocky summits provide more stable monuments than do boggy lowland soils.

1.3 VLBI

Very Long Baseline Interferometry (VLBI) measures the position of radio antennas with respect to radio sources in quasars (Smith and Turcotte, 1993). Although capable of sub-millimeter precision in relative position vectors (Herring, 1992), this technique requires large (~ 10 m) antennas. As such, it has only measured coseismic displacements for a few earthquakes: Loma Prieta, California (Clark *et al.*, 1990), and the 1987–1988 Gulf of Alaska earthquakes (Sauber *et al.*, 1993).

Nonetheless, VLBI supports earthquake studies by contributing important geometric information to the definition of geodetic reference systems such as the International Terrestrial Reference Frame (ITRF) (Sillard *et al.*, 1998).

1.4 SLR

Satellite laser ranging (SLR) measures the round-trip distance between an instrument on the ground and a reflective, massive, spherical satellite in low (500–1200 km altitude) orbit. The measurement uncertainty is typically 7 cm in distance, which implies subcentimeter uncertainties in all three vector components of relative position between two benchmarks (Tapley *et al.*, 1993). Since SLR instruments are many times heavier than for GPS, they are usually deployed at astronomic observatories, with the exception of a few mobile instruments deployed in California under the auspices of NASA's Crustal Dynamics Program (CDP) marks (Smith and Turcotte, 1993) and in the Mediterranean region under the WEGENER program (Smith *et al.*, 1994; Noomen *et al.*, 1996). In both of these networks, most of the SLR measurements useful for tectonic studies occurred in the late 1980s and have been largely supplanted by GPS in the 1990s. As a result, I could not find a published example of a coseismic displacement recorded by SLR.

1.5 GPS

The Global Positioning System (GPS) can provide subcentimeter estimates of relative position using an instrument available for less than “10 kg, 10 W, and 10 \$K.” Since the most precise solutions involve postprocessing data from multiple instruments, it typically requires several days between acquisition and estimate. The constellation of satellites came into use gradually beginning in 1985; it became fully operational in 1992. Data from this early period are typically more difficult to analyze and may yield less precise results than more recent surveys. For reviews of geophysical applications, see Dixon (1991), Hager *et al.* (1991), Hudnut (1995), Larson (1995), and Segall and Davis (1997). For earthquake studies, GPS networks tend to operate in one of two end-member modes: continuous operation of permanently installed, widely spaced antennas (CGPS), or intermittent occupation of densely spaced benchmarks in “campaign” mode. The former offers good temporal resolution (1 measurement/30 seconds = 33 mHz) but poor spatial resolution (>100 km between stations), whereas the latter offers poor temporal resolution (1 measurement/year = 32 nHz) and good spatial resolution (~10 km between stations). This trade-off between temporal and spatial resolution creates a difficult decision in the face of limited resources. Although a compromise “hybrid” strategy could rotate expensive receivers on a roughly monthly basis through several fixed monuments, this approach has yet to be

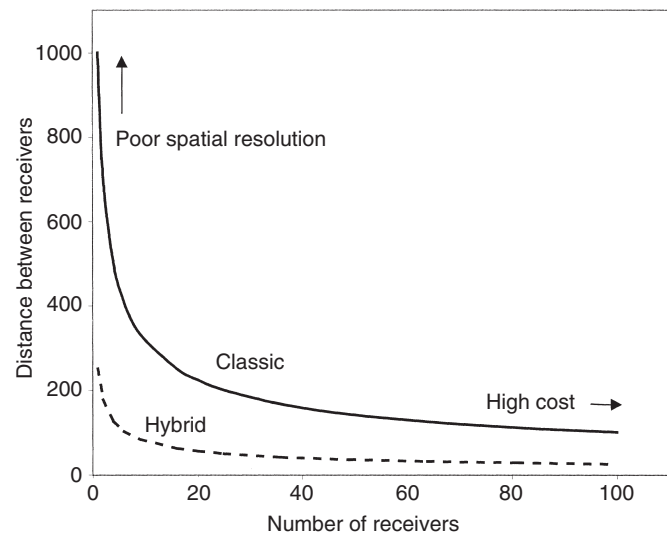


FIGURE 2 Tradeoff between poor spatial resolution and high cost in a GPS network designed to cover an area $a^2 = 1000$ km by 1000 km with n instruments spaced d km apart implies that $d = a/n$. Permanently deploying one receiver at each benchmark in the network in the “classic” approach (solid line) costs more than rotating each receiver through (say) four sites in the “hybrid” approach (dashed line).

deployed, apparently because it requires more manpower than do permanent installations (Fig. 2).

1.6 DORIS

Détermination d'Orbite et Radiopositionnement Intégré par Satellite (DORIS) is a Doppler satellite navigation system developed by the French Space Agency (Lefebvre *et al.*, 1996). Designed for tracking satellites in orbit, this system currently flies on three satellites (SPOT2, SPOT4 and Topex/Poseidon). It resembles GPS with three important differences. First, the transmitter is on the ground, not on the satellite. Second, the current design of the space-borne receiver cannot track more than three instruments on the ground within a radius of 1000 km, although this restriction will be relaxed with a new design to be launched aboard Jason in 2000. Third, the current DORIS tracking network covers the globe quite well, with at least one station on each of the 11 lithospheric plates.

These differences imply that DORIS is better suited to measuring plate motions at the global scale than is GPS, which still suffers from a lack of long-term stations in the southern hemisphere. For this application, multiyear time series of DORIS data can determine absolute velocities with uncertainties of $1\text{--}2\text{ mm y}^{-1}$ in horizontal components (Créaux *et al.*, 1998).

On the other hand, DORIS is less well suited to local studies of earthquakes and faulting at scales shorter than 1000 km than is GPS, although the station at Sakhalin did capture the 1994

earthquake in Kamchatcka (A. Cazenave, personal communication, 1999).

1.7 SAR Interferometry

This geodetic technique calculates the interference pattern caused by the phase difference between two images acquired by a space-borne synthetic aperture radar (SAR) at two distinct times. The resulting interferogram is a contour map of the change in distance between the ground and the radar instrument. Each fringe represents a range change of half the wavelength. Thus, the contour interval is 28 mm for C-band radars such as ERS and RADARSAT and roughly four times larger, 125 mm for the L-band JERS satellite. These maps provide an unsurpassed spatial sampling density (~ 100 pixels km^{-2}), a competitive precision (~ 1 cm) and a useful observation cadence (1 pass/month), as described in a review article by Massonnet and Feigl (1998), which is paraphrased here.

To capture an earthquake, INSAR requires three data sets: a SAR image before the earthquake, one after, and topographic information. The SAR images themselves are rich data sets well documented in the remote sensing literature (Curlander and McDonough, 1991; Henderson and Lewis, 1998).

The topographic information is necessary to model and remove the interferometric fringes caused by topographic relief as “seen in stereo” from slightly different points of view. To handle the topographic contribution, we can choose between the “two-pass” approach (e.g., Massonnet and Feigl, 1998) and the “three-pass” or “double-difference” approach (e.g., Zebker *et al.*, 1994). For earthquake studies, there is usually a trade-off between the two-pass approach, which requires a digital elevation model (DEM), and the three-pass approach, which requires a third SAR acquisition. Further discussion of relative merits of the two- and three-pass approaches are beyond the scope of this chapter.

To interpret an interferogram, one must understand how different effects contribute to the fringe pattern. Many instructive examples appear in review papers by Massonnet and Feigl (1998) and Madsen and Zebker (1998). The mathematical details appear in another review (Bamler and Hartl, 1998). For earthquake studies, the most important effects involve topographic relief, orbital trajectories, and tropospheric refraction, usually in combination.

If the topographic information (a DEM for two-pass, or the “topo pair” in three-pass INSAR) is in error, the interferogram will contain artifactual fringes. They appear in the same location in every interferogram produced using that topographic model. To quantify this effect, Massonnet and Rabaute (1993) define the altitude of ambiguity h_a as the shift in altitude needed to produce one topographic fringe. Indeed, this parameter is inversely proportional to the perpendicular component of the (“baseline”) vector separating the two orbital trajectories, conventionally written B_{\perp} , pronounced “*B*-perp,” and given in

meters (Zebker and Goldstein, 1986). The number of “topographic” fringes is proportional to B_{\perp} and inversely proportional to h_a . Thus we seek pairs of orbital trajectories with a small separation, that is, with *small* (absolute) values of B_{\perp} and *large* (absolute) values of h_a for earthquake studies. It turns out that for the ERS satellites, an acceptably good orbital pair has both B_{\perp} and h_a approximately equal to 100 m.

A topographic error of ε meters in the DEM will produce a phase error of ε/h_a fringes in the resulting interferogram. Errors in typical DEMs range from 10 to 30 m (Wolf and Wingham, 1992), implying that choosing a pair of images with $|h_a|$ between 20 and 60 m will yield an interferometric measurement with an error better than $\varepsilon/h_a = \pm 1/2$ cycle, or ± 14 mm for ERS. Small values of $|h_a|$ can mask even large signals with artifactual topographic fringes. In an extreme (and rare) case, Massonnet and Feigl (1995a) uncovered a topographic error of $\varepsilon \sim 250$ m, roughly 8 times larger than the published precision for the DEM. This artifact resembles the fringe pattern produced by a small earthquake. Avoiding such confusion requires looking at several interferograms with different values of h_a . For an earthquake, the number of coseismic fringes does not depend on h_a .

Atmospheric effects can also complicate the interpretation of an interferogram. Indeed, variations in the refractive index of the troposphere are the current limiting source of error in the INSAR technique (Goldstein, 1995; Massonnet and Feigl, 1995a; Rosen *et al.*, 1996; Tarayre and Massonnet, 1996; Zebker *et al.*, 1997; Hanssen, 1998). Potentially, one could confuse a topographic signature with a displacement, if propagation effects create fringes which “hug” the topography like contour lines, but which measure the change in tropospheric delay. This effect was first observed as several concentric fringes in a 1-day interferogram on Mt. Etna (Massonnet and Feigl, 1998; Beauducel *et al.*, 2000). One can recognize this subtle effect using pairwise logic (Massonnet and Feigl, 1995a) or using a DEM and local meteorological observations (Delacourt *et al.*, 1998; Williams *et al.*, 1998). However, separating the tropospheric noise from the deformation signal can be challenging, particularly when the signal is small, e.g., the magnitude 5.2 earthquake near St. Paul de Fenouillet, France (Rigo and Massonnet, 1999).

1.8 Correlation of Two Remote-sensing Images

It is also possible to detect (large) coseismic displacements by correlating two optical images. The “lag” vectors estimated between the corresponding subpixel cells of a prequake and a postquake image yields the horizontal components of the coseismic displacement vector with meter-level precision and hectometer resolution (Crippen, 1992; Crippen and Blom, 1992). The same technique also applies to SAR images. By correlating two Single Look Complex (SLC) SAR amplitude (“backscatter”) images acquired at different times, Michel *et al.*

(1999) measured ground displacements for the Landers earthquake. Their result is “a two-dimensional displacement field with independent measurements every about 128 m in azimuth and 250 m in range. The accuracy depends on the characteristics of the images. For the Landers test case discussed in the study, the 1- σ uncertainty is 0.8 m in range and 0.4 m in azimuth. [They] show that this measurement provides a map of major surface fault ruptures accurate to better than 1 km and an information on coseismic deformation comparable to the 92 GPS measurements available. Although less accurate, this technique is more robust than SAR interferometry and provides a complementary information since interferograms are only sensitive to the displacement in range.” (Michel *et al.*, 1999.)

2. Estimating Earthquake Parameters by Inversion of Geodetic Data

2.1 The Standard Elastic Half-space Model

To explain the observed coseismic deformation, a simple model of a dislocation in an elastic half-space provides a good approximation. Indeed, it has become the conventional model used in most of the case studies considered here. Okada (1985) derives the expressions for the coseismic (permanent) displacement u at the Earth’s surface caused by a fault at depth in closed analytic form. Accordingly, the displacement field $u_i(x_1, x_2, x_3)$ due to a dislocation $\Delta u_j(\xi_1, \xi_2, \xi_3)$ across a surface Σ in an isotropic medium is

$$u_i = \frac{1}{F} \int_{\Sigma} \int \Delta u_j \left[\lambda \delta_{jk} \frac{\partial u_i^n}{\partial \xi_n} + \mu \left(\frac{\partial u_i^j}{\partial \xi_k} + \frac{\partial u_i^k}{\partial \xi_j} \right) \right] v_k d\Sigma \quad (1)$$

where δ_{jk} is the Kronecker delta, λ and μ are Lamé’s coefficients, v_k is the direction cosine of the normal to the surface element $d\Sigma$, and the summation convention applies. The term u_i^j is the i th component of the displacement at (x_1, x_2, x_3) due to the j th direction point force of magnitude F at (ξ_1, ξ_2, ξ_3) . For the complete set of equations see Okada (1985), who also corrects previous derivations. A public-domain computer program performs these calculations (Feigl and Dupré, 1999). Called RNGCHN, this program is included on the Handbook CD-ROM under the directory \37Feigl (see Chapter 85.19 for a brief description). Okada (1992) performs this calculation at any point in the half-space.

2.2 Fault Parameters

Here I follow Okada’s (1985) notation, as in Feigl and Dupré (1999). To describe a single fault element (also called a “sub-fault” or “patch”) as a dislocation requires ten parameters. The fault patch has length L and width W . The slip on the fault plane

is a vector \mathbf{U} with three components, U_1 , U_2 , and U_3 . The position coordinates of the fault patch are E , N , and d , taken positive east, north, and down. The azimuth α gives the strike of the fault, in degrees clockwise from north. Finally, an observer facing along strike should see the fault dip at δ degrees to his right.

The Okada parameters differ slightly from the parameters favored by seismologists. In particular, the origin of Okada’s fault patch does not coincide with the centroid at the geometric center of the fault rectangle (Feigl and Dupré, 1999). For a double-couple source, the tensile component vanishes ($U_3=0$) and the slip vector \mathbf{U} lies in the fault plane. Seismologists define the rake angle r such that $\tan r = U_2/U_1$ (Aki and Richards, 1980). Inversely, $r = \text{ATAN2}(U_2, U_1)$ where ATAN2 is the usual FORTRAN intrinsic function for arctangent (U_2/U_1) on the range $[-180^\circ, +180^\circ]$. A thrust-faulting mechanism, for example, has $U_2 > 0$ and $r > 0$. A normal faulting mechanism, on the other hand, has $U_2 < 0$ and $r < 0$. Similarly, left-lateral slip implies $U_1 > 0$ and $|r| \leq 90^\circ$, whereas right-lateral slip implies $U_1 \geq 0$ and $|r| \geq 90^\circ$.

2.3 Underlying Assumptions

The standard Okada model assumes that the Earth’s surface is flat, corresponding to the bounding plane of the elastic half-space. The Lamé coefficients λ and μ specify the elastic medium. For simplicity, most studies assume that $\lambda = \mu$, so that these parameters drop out of the expressions for surface displacement. Such a medium, called a Poisson solid, has a Poisson’s ratio of 1/4, a reasonable approximation to the values of 0.23–0.28 estimated from P - and S -wave velocities in the upper crust (Perrier and Ruegg, 1973; Dziewonski and Anderson, 1981). The so-called “geometric moment” or “potency” simply equals ULW . To obtain the seismic moment, multiply by the shear modulus μ so that $M_0 = \mu ULW$. Typical values (assumed) for μ in the Earth’s crust range from 30 to 36 GPa, but values as low as 10 GPa (Dal Moro and Zadro, 1999) and as high as 50 GPa (Barrientos and Ward, 1990) have been used. The simplest assumption takes this value to be constant throughout the half space, although some authors propose increases with depth (Dolan *et al.*, 1995; Cattin *et al.*, 1999). Some authors call μ the “rigidity,” whereas others use μ to denote a dimensionless coefficient of friction. To convert moment into the various magnitude scales, use the conventional formulas (Hanks and Kanamori, 1979; Abe, 1995). Empirical relations exist for establishing the size (L , W , and U) of the earthquake from the seismological magnitude or moment (Scholz, 1990; Dolan *et al.*, 1995).

2.4 Particularities of Geodetic Data

Like seismograms, geodetic measurements decompose the displacement vector into components. Although VLBI and GPS both record three components of the coseismic displacement

vector (postquake minus prequake position) of a benchmark, INSAR records only the component along the line of sight between the satellite and ground point. Image correlation provides the same line-of-sight (range) component as well as a second component parallel to the satellite trajectory (azimuth). The line of sight between the point on the ground and the radar satellite in the sky defines two angles, the radar incidence (from vertical) and the azimuth of the satellite ground track (from North). For the ERS satellites in California, for example, these quantities are approximately 23° and 13° , respectively. These quantities determine the unit vector \hat{s} which points from ground to satellite. Then the change in range $\Delta\rho$ or the distance measured along the line of sight between the satellite and ground point is

$$-\rho = \mathbf{u} \cdot \hat{s} \quad (2)$$

Note that the sign convention is such that an upward movement will produce a positive value of $\mathbf{u} \cdot \hat{s}$, a decrease in range, and a negative value of $\Delta\rho$. The ray specified by $-\hat{s}$ is sometimes called the “look vector.” INSAR can provide a second component of the coseismic displacement vector if the satellite acquires two images in both the “ascending” (south-to-north) and “descending” (north-to-south) orbital passes. In this case, the east, north, and upward components of the unit vector \hat{s} are $[x, y, z]$ and $[x, -y, z]$, respectively. To use the radar interferograms as data in an inverse problem requires an unambiguous measurement of the range change, which implies “unwrapping” the interferogram. See Ghiglia (1998) for a review of the techniques involved. For the Landers and Fawnskin earthquakes described below, we simply count and digitize the fringe pattern. Although tedious, this technique avoids errors because the human eye is very good at following colored fringes, even where they are noisy. It also recognizes areas where the fringes become too noisy to count. For the Eureka earthquake, a straightforward algorithm (Tarayre, 1994) performed well because the fringes were clear and simple.

Even unwrapped, radar range changes are still only relative measurements. To make them absolute, we must identify the fringe corresponding to zero deformation. We can do this by trial and error (Feigl *et al.*, 1995), or explicit estimation (Wright *et al.*, 1999), choosing the additive constant which produces the smallest misfit to the observed interferogram. Usually, the null fringe intersects the fault plane.

2.5 Modeling by Trial and Error

The standard Okada model defines the relation between the earthquake source parameters and the geodetic measurements of surface displacement. The goal is to find the values of parameters which best fit the data. This inverse problem seeks to minimize the difference between the modeled displacement field and the one sampled by geodesy. The simplest procedure is trial and error, usually called “forward modeling.” We use

our best guess for the value of each parameter to calculate a synthetic displacement field. With some clues about the location, geometry, and magnitude of the earthquake, it is not difficult to find a simulation which looks like the observed displacement field. By repeatedly tuning the parameters, we can usually fit the data better than our first guess. This procedure provided the first approximation to the coseismic deformation in most of the studies listed in Table 1.

2.6 Estimating the Focal Mechanism

If we choose to estimate all ten parameters for a single fault patch, the problem is nonlinear because the surface displacement depends strongly on the fault geometry. The approach uses “numerical optimization procedures to determine the best-fitting dislocation surface or surfaces. The methods can generally be divided into two categories: those methods, such as nonlinear least squares or quasi-Newton methods, that make use of the first or second derivatives and Monte Carlo methods that do not require these derivatives,” as described by Segall and Davis (1997).

For the derivative-based methods, the RNGCHN program includes analytic expressions for the first derivatives. These allowed us to use an iterative linearized least squares procedure for the 1992 Fawnskin (Feigl *et al.*, 1995) and 1993 Eureka Valley earthquakes (Massonnet and Feigl, 1995b).

The Monte Carlo techniques have the advantage of avoiding local minima and furnishing realistic estimates of uncertainties, as shown for the Loma Prieta (Arnadottir and Segall, 1994) and Cape Mendocino (Murray *et al.*, 1996) earthquakes.

Mixing the two categories of optimization methods in a hybrid, Monte-Carlo, downhill simplex scheme also works (Clarke *et al.*, 1996, 1998; Wright *et al.*, 1999).

2.7 Surface Rupture by Earthquake Faulting

By definition, a mapped fault is a discontinuity separating two blocks of the Earth’s crust. If the fault is active, the relative motion (slip) between the two blocks offsets the interferometric fringe pattern. Thus, surface rupture appears as a discontinuity in an interferogram, except where the slip vector is orthogonal to the radar look vector. Offsets as small as a centimeter tear the fringe patterns at Landers (Massonnet *et al.*, 1994; Price and Sandwell, 1998), Hector Mine (Sandwell *et al.*, 2000), and in the South Iceland Seismic Zone (Feigl *et al.*, 2000).

2.8 Fault Slip

Once we know the geometry of the fault, we can estimate the distribution of the slip vector \mathbf{u} . This inverse problem is linear. The components of the surface displacement \mathbf{U} are proportional to the components of the slip vector \mathbf{u} . As such, it is simple to divide the modeled fault plane into many discrete patches. By varying only the amount of slip on each patch, but not its

geometry, we can estimate the distribution of slip on the fault plane. Numerous published examples of this procedure are listed in Table 1. Although most authors approach this problem using discrete fault patches, Bennett *et al.* (1994) use continuous functions. Comparing different solutions to this inverse problem is hindered by the lack of a single standard format for computer files. Worse still, very few authors publish the centroid of their estimate.

2.9 Moment

Geodetic observations of coseismic displacement are difficult to obtain because they require a measurement before the earthquake. Furthermore, such measurements are only possible at the Earth's surface. As a consequence, geodetic data sets tend to be sparse. To extract the most information from these data sets, we want to limit the number of free parameters in the optimization. Taken to the extreme, this approach suggests estimating only a single parameter — the moment — from the available data, as Johnson *et al.* (1994) do for the Landers earthquake.

2.10 Data Covariance Matrix

In solving these inverse problems, we expect to find a more reliable solution and a better estimate of the uncertainties if we account for the full covariance matrix, including the off-diagonal terms of the data. The Loma Prieta earthquake provides a case in point. There, Marshall *et al.* (1991) and Lisowski *et al.* (1990) applied standard least squares methods to the leveling and trilateration data, respectively, neglecting the off-diagonal elements of the data covariance matrix. As a result, they had to resort to a two-patch model to fit the geodetic data. This model came under fire because the second patch did not pass through the locus of aftershock hypocenters. By including the full covariance matrix, however, Arnadottir *et al.* (1992) were able to find an acceptable single-patch model which also fitted the aftershock distribution. The same authors later improved on their first model by allowing the slip to vary in a bootstrap Monte Carlo approach (Arnadottir and Segall, 1994).

Complete knowledge of the data covariance matrix is also necessary in joint inversions to weight the different types of data (Barrientos and Ward, 1990; Holdahl and Sauber, 1994).

3. Case Studies

3.1 Loma Prieta, California, 1989

In addition to revealing the importance of using the covariance matrix when inverting geodetic data, the Loma Prieta earthquake also focused attention on the issue of postseismic deformation. To fit the geodetic observations, Savage *et al.* (1994) proposed a model of “fault collapse” such that the

dislocation included a (negative) tensile component akin to reducing the volume of a rectangular prism or dike. Arnadottir *et al.* (1992) later concluded that the “geodetic data do not place useful constraints on the amount of dilatancy for this event,” a conclusion reaffirmed later (Bürgmann *et al.*, 1997).

3.2 Landers, California, 1992

Color Plate 14 shows INSAR results for the 1992 Landers earthquake. The slip distribution estimated from the radar data [shown in Plate 21 of Massonnet and Feigl (1998)] agrees qualitatively with those estimated from GPS survey measurements of coseismic displacements (Murray *et al.*, 1993; Freymueller *et al.*, 1994; Hudnut *et al.*, 1994), strong motion accelerations recorded in the near field (Cohee and Beroza, 1994; Cotton and Campillo, 1994, 1995), seismograms in the far field (Wald and Heaton, 1994), a joint inversion of all three data types (Wald and Heaton, 1994), and a combination of INSAR and strong motion data (Hernandez *et al.*, 1997, 1999). All these inversions find relatively little slip (2–3 m) below the epicenter where rupture began, but a maximum of 8–12 m of slip located at 5–10 km depth in the Homestead and Emerson fault segments between 30 and 40 km north of the epicenter. The depth and magnitude of the slip maximum seems to depend on the prior information in the various inversions. All the estimates agree on the seismic moment, in accord with the centroid moment tensor and the bounds estimated from the geodetic data (Johnson *et al.*, 1994).

The estimates of slip distribution contributed to calculations of coseismic stress changes which load the crust and thus trigger subsequent earthquakes (Harris and Simpson, 1992; Jaumé and Sykes, 1992; Stein *et al.*, 1992). By using a fine estimate of slip distribution estimated from several data sources (Wald and Heaton, 1994), Stein *et al.* (1994) predict aftershock locations better than with their original calculation (Stein *et al.*, 1992) which used only a coarse estimate of slip distribution based on GPS measurements alone (Murray *et al.*, 1993).

Both GPS and INSAR also measured postseismic deformation following this earthquake (Massonnet *et al.*, 1994; Shen *et al.*, 1994; Wyatt *et al.*, 1994; Massonnet and Feigl, 1995a; Massonnet *et al.*, 1996b; Peltzer *et al.*, 1996, 1998; Bock *et al.*, 1997; Savage and Svarc, 1997; Pollitz *et al.*, 2000), but these observations and the models needed to explain them exceed the limits of this chapter.

3.3 Eureka Valley, California, 1993

The Eureka Valley earthquake occurred on 17 May 1993 in a remote area of the Mojave Desert at the edge of the Basin and Range province. The normal-faulting $M_w = 6.1$ mainshock and subsequent aftershocks deepened the graben in an oval-shaped coseismic deformation field. The ERS-1 radar images are the only available geodetic measurements. This earthquake is an

interesting case study because two different approaches led to different interpretations. Massonnet and Feigl (1995b) calculate this interferogram by stacking two 2-pass interferograms in a combination of three radar images. Peltzer and Rosen (1995) analyze the same three images with the 3-pass technique. Both studies find approximately 10 cm of range increase.

To explain the observed fringe pattern, Massonnet and Feigl use an iterative least-squares procedure and the standard elastic dislocation model to estimate the earthquake focal mechanism. The best-fitting focal mechanism is a normal fault dipping $54^\circ \pm 2^\circ$ to the west and striking $S7^\circ W \pm 2^\circ$. The 16×7 km rectangular fault patch centered at 9 km depth does not cut the surface. The estimated geodetic moment magnitude of 6.1 agrees with the seismological estimates from wave-form inversion. The residual interferogram shows less than one 14 mm cycle in the difference between the observed and modeled fringes.

The location of the centroid estimated from the radar data is less than 6 km horizontally and 2 km vertically from the hypocenter estimated from *P*-wave travel times. The modeled fault patch, however, strikes more westerly than the mapped Quaternary fault or the fault plane estimated from first motions. Indeed, Peltzer and Rosen find that a fault plane striking $N7^\circ E$, dipping 50° west, but cutting the surface, provides a good fit to their radar interferogram, based on forward modeling. The fault patch estimated by Massonnet and Feigl resembles the locus of aftershocks in dip, length, width and horizontal location, but not depth.

The fault models also disagree about the depth of the slip, in particular, whether or not it breaks the surface. Peltzer and Rosen favor a variable-slip (multi-patch) fault model in which the uppermost fault patches cut the surface, while Massonnet and Feigl's optimized 1-patch model stops some 6 km short of the surface. Furthermore, Peltzer and Rosen observe an offset of approximately 3 cm in their interferogram, whereas Massonnet and Feigl see no such discontinuity longer than 1 km in their interferogram. Furthermore, Peltzer and Rosen observed a fault scarp with 1–3 cm of vertical displacement which they could follow in the field for a few tens of meters. Any surface rupture would have to be small, both in magnitude and spatial extent, to avoid cutting the fringes observed in Massonnet and Feigl's interferogram.

A small, shallow aftershock can explain all the observations and resolve the controversy. Some 3 cm of slip on a fault 1 km^2 in area represents an earthquake of magnitude 4. An earthquake of approximately this magnitude ($M_L = 3.5$) occurred at 0.02 km depth in this area. This location is also less than 1 km from the offset observed by Peltzer and Rosen, well within the uncertainties of the seismological estimates. Such an earthquake could have produced the short scarp observed by Peltzer and Rosen in the field. It could also produce concentric fringes 1 or 2 km in diameter in the interferogram. Two such fringes (28 mm of range) are

barely discernible near its epicenter in Massonnet and Feigl's interferogram.

3.4 Grevena, Greece, 1995

A $M_s = 6.6$ normal-faulting event in northern Greece illustrates the complexity of estimating source parameters from diverse data sets with different data types. The earthquake occurred near Kozani–Grevena on 13 May 1995, a decade after a triangulation survey, almost two years after the prequake ERS image, and 3–7 days before the field observations of centimeter-scale surface breaks. These observations form the basis of two separate analyses of the coseismic deformation which differ markedly both in their approaches and in their conclusions. Clarke *et al.* (1996) used GPS after the earthquake to measure 91 concrete pillars that had been surveyed prior to the earthquake by triangulation with formal uncertainties of 15 mm in horizontal relative position. Using a “hybrid simplex-Monte Carlo method which requires no a priori constraints,” they estimate the focal parameters for a single fault patch. Working separately, Meyer *et al.* (1996) used INSAR to calculate several coseismic interferograms. The best one spans almost two years and is only partially coherent. Using the INSAR results in conjunction with their map of surface rupture, tectonic maps of fault geometry, Meyer *et al.* (1996) determine a model with 22 fault patches.

The two models disagree substantially, leading to a critical exchange of comment (Meyer *et al.*, 1998) and reply (Clarke *et al.*, 1998). The GPS-derived model predicts coseismic INSAR range changes that disagree with the observed interferogram. Similarly, the INSAR-based model predicts coseismic displacements that disagree with the displacements observed by the GPS-triangulation comparison by more than several times their measurement uncertainty. There are several partial explanations for this discrepancy.

Firstly, the two studies invert data which sample the coseismic displacement field in different places. The INSAR coherence breaks down in several crucial areas: both where Meyer *et al.* could measure surface rupture and around many of the pillars where Clarke *et al.* measured large displacements. And the spatial distribution of the data makes a difference in the inversion procedure, as discussed below.

Secondly, the inversion procedure makes a difference, as described in the comment and reply. In particular, constraining the fault plane to pass through the mapped surface break can shift the fault plane significantly, particularly in the presence of irregularly sampled data.

This exercise of independent analyses of independent data sets raises several issues. First, that geodetic and seismological estimates of moment can differ significantly. Second, we still lack good ground-truth evaluations of surface breaks as measured by INSAR, which records them as discontinuities in the fringe pattern. Thirdly, the geometric relationship between geodetically estimated fault planes, the

mainshock location, and the distribution of aftershocks is not clear.

4. Synthesis and Conclusions

4.1 Depth Estimates

Several studies suggest that geodetic estimates tend to locate the coseismic slip at a shallower depth than seismological estimates of the mainshock hypocenter or centroid. There are several possible explanations for this discrepancy which became glaringly apparent for the Northridge earthquake (Hudnut *et al.*, 1995).

4.1.1 Rheological Inhomogeneity

For computational simplicity, most geodetic inversions assume an elastic half-space with a constant rheology throughout. Local heterogeneities in crustal rheology clearly violate this assumption. The half-space approximation is not even consistent with the simple layered models routinely used for locating earthquake hypocenters. In particular, if the assumed value of the shear modulus μ is too high, then the geodetic estimate will underestimate the depth, yielding a location which is too shallow (Cattin *et al.*, 1999). This shortcoming may also explain the observation that most of the aftershocks are near, but not on, the mainshock fault plane for Northridge (Hudnut *et al.*, 1995), Cape Mendocino (Murray *et al.*, 1996), and Antofagasta, Chile (Ruegg *et al.*, 1996). Thus Segall and Davis (1997) suggest that “it now seems probable that the effects of inhomogeneity, and perhaps anisotropy in the Earth’s crust can no longer be neglected (e.g., Du *et al.*, 1994).” A different solution to this problem allows layering in a spherical earth (Pollitz, 1996; Cummins *et al.*, 1998). The differences with respect to the half-space solution can be of the order of 10–20% at distances of 100–400 km from the source (Cummins *et al.*, 1998).

4.1.2 Nonplanar Fault Geometry

A normal fault which shallows with depth, as Meyer *et al.* (1996, 1998) argue for Grevena, is difficult to approximate with the simple model of a single, planar fault patch. Since the latter is the only feasible geometric parametrization in the nonlinear focal mechanism inverse problem, it may not pass through the mainshock hypocenter unless constrained to do so (Clarke *et al.*, 1996, 1998).

4.1.3 Irregular Distribution of Data

Geodetic networks with benchmarks on rock outcrops do not form regular grids. Even INSAR, which in principle samples the deformation on a regular grid, can break down in certain areas, creating “blots” of missing data. For the Dinar earthquake, for example, all the usable INSAR data fall on the

hanging-wall block (Wright *et al.*, 1999). Such an asymmetric distribution of data may tend to “pull” the modeled fault plane towards the data points so that it does not pass through the mapped surface rupture unless constrained to do so (Wright *et al.*, 1999).

4.2 Distribution of Slip and Aftershocks

The Landers studies show that aftershocks tend to occur near the parts of the fault plane where the amount of slip is small, e.g., Plate 21 of Massonnet and Feigl (1998) and Figure 13 of Cohee and Beroza (1994). In other words, aftershocks correlate spatially with the absence of slip. A similar, but weaker, correlation has also been observed for Loma Prieta (Arnadottir and Segall, 1994). It seems that slip may relieve stress on the fault patch where it occurs, but increase stress in neighboring patches.

4.3 Geodetic Versus Seismological Estimates of Moment

Figure 3 shows that geodetic estimates of seismic moment tend to exceed seismological estimates by as much as 60%. Again, there are several possible explanations.

4.3.1 Measurement Interval

Geodetic measurements of relative position before and after the earthquake span a much longer period of time than does a seismogram and thus include more deformation, both interseismic and postseismic. Thus geodetic measurements sometimes include the moment released by aftershocks and/or afterslip, whereas the seismological estimate pertains only to the mainshock (Kanamori, 1973; Wyatt, 1988). Whereas historical geodetic measurements may impose an interval of several decades, satellite techniques can reduce the interval to a single 35-day orbital cycle in the case of the ERS satellites or to a single day or less in the case of continuous GPS. In this sense, geodesy, as ultralong period seismology, should follow the rule of thumb that moment estimates tend to increase with the measurement period.

4.3.2 Incorrect Shear Modulus

To convert seismic potency (in m^3) to moment (in N m) requires accurate knowledge of the shear modulus μ . Yet this parameter is rarely measured. Usually, it is assumed to take conventional values between 30 and 36 GPa, a range large enough to explain a 20% discrepancy. Of course, for a rigorous comparison, we should use the same value for the shear modulus μ in the (geodetic) dislocation model and in the (seismological) velocity model. In practice, however, this will require generalizing the dislocation theory to admit layering.

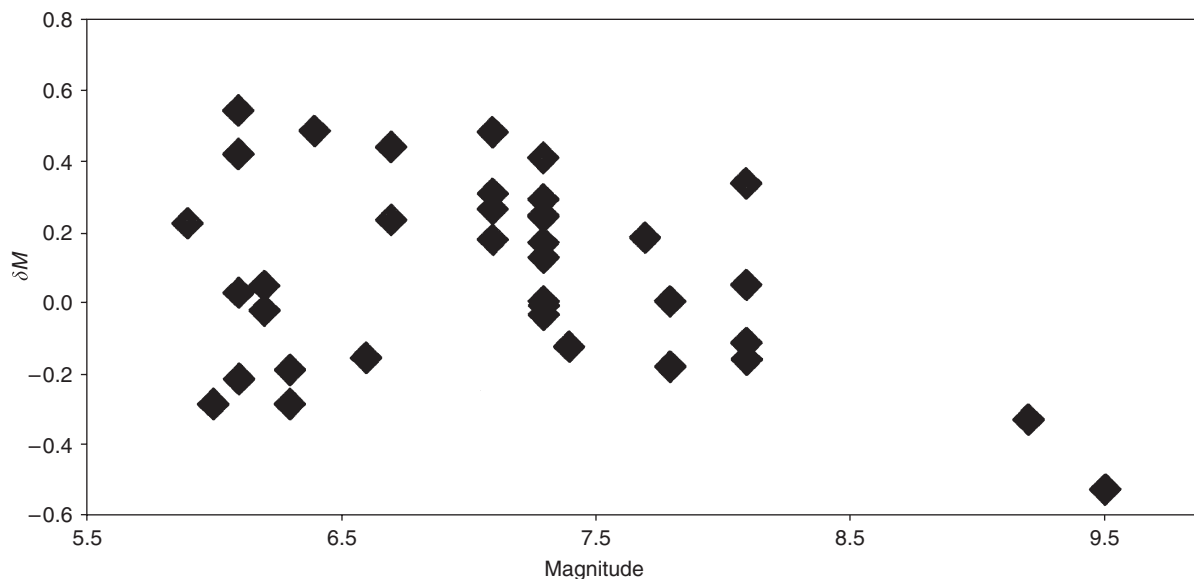


FIGURE 3 Comparison of seismic moment estimated from geodetic measurements $M_0^{(g)}$ and seismic moment estimated from centroid moment tensor solutions $M_0^{(s)}$. The vertical axis shows the ratio $\delta M = (M_0^{(g)} - M_0^{(s)})/M_0^{(s)}$ using the values in Table 1. The geodetic moment is larger than the seismic moment for most events.

4.3.3 Aseismic Deformation

Geodetic estimates of moment will include deformation caused by any phenomenon including creep, fluid injection, or even “silent” earthquakes. For example, the geodetic estimate derived from the 2 m of displacement measured for the 1978 Asal rifting event in the Afar region is 6×10^{17} N m, over three times larger than the 1.7×10^{17} N m estimated for the sum of the two largest $M = 5$ earthquakes (Lépine *et al.*, 1979; Ruegg *et al.*, 1979; Stein *et al.*, 1991).

4.4 Conjugate Faults

For earthquakes of intermediate magnitude, choosing between two possible focal planes is both challenging and interesting. For a point source observed from the far field, neither seismological analysis of first arrivals nor geodetic measurements of surface displacements can tell the difference because the two cases produce rigorously identical results. For example, a fault plane parallel to the subduction zone and a plane perpendicular to it both fit the large coseismic displacements observed by continuous GPS after the 1994 Hokkaido-Toho-Oki earthquake in Japan (Tsuji *et al.*, 1995).

For a dipping, finite fault with dimensions larger than the distance between geodetic observations, this ambiguity should fade as asymmetry begins to appear. In particular, the displacement vectors above the downdip edge of the fault are smaller than above the upper edge. In some cases, the RMS misfit is less than 1 mm better for one fault plane than for its conjugate (Stein *et al.*, 1991; Feigl *et al.*, 1995; Massonnet and

Feigl, 1995b). With good sampling, however, it is possible to identify the rupture plane (Hudnut *et al.*, 1995).

4.5 Utility for Assessing Seismic Risk

Since seismologic data yield good estimates of the slip distribution, why estimate it from geodetic data? In remote areas, strong-motion seismological instruments may not exist, whereas a satellite radar interferogram can provide true remote sensing. Second, geodetic surveys record deformation over a much longer period (several months), than the seismological record, revealing any slip which occurred before or after the mainshock rupture. Third, geodetic surveys can capture aseismic slip. Finally, accurate descriptions of the total slip distribution are useful for calculations of coseismic stress changes.

4.6 Future Prospects

To contribute more useful information to the understanding of earthquake source parameters, geodetic analyses should attempt to address the following issues.

4.6.1 Measurement Uncertainty for INSAR

We do not yet understand know the error budget for INSAR measurements. For sophisticated inversion schemes, we should account for the structure of the data covariance matrix. This issue becomes particularly important for joint inversions of different data types, such as INSAR with GPS, or strong-motion seismograms. I emphasize that correlations between data also

influence Monte Carlo-like algorithms, which often incorrectly assume independent, random data.

4.6.2 Routine Application of INSAR

To date, several factors make INSAR measurements of coseismic deformation a hit-or-miss, opportunistic affair. For example, the lack of a good digital elevation model can inhibit the application of INSAR to earthquakes outside the US. This difficulty should be resolved by the Shuttle Radar Topography Mission flown in early 2000. Its data should lead to public distribution of a 90 m DEM by 2004. Similarly, the lack of closely spaced orbital trajectories can force compromises. This difficulty will be partially alleviated by ENVISAT, which will have better orbital control than ERS, JERS, or RADARSAT. Third, capturing earthquakes with INSAR is a major challenge because no-one knows where they will occur. This implies that each INSAR-capable satellite must acquire a catalog of pre-quake images over all the land areas likely to produce a measurable earthquake. I estimate this area to be approximately 66 million km².

4.6.3 Joint Inversions

Geodetic data seem to help constrain seismological solutions at relatively long temporal periods (days to years) and intermediate spatial scales (within several fault dimensions of the rupture), as demonstrated for Landers by Wald and Heaton (1994). They inverted GPS measurements of coseismic displacements, strong motion seismograms and teleseismic wave forms, both jointly and separately. Including INSAR measurements in this type of inversion is likely to furnish interesting results, as suggested for Landers (Hernandez *et al.*, 1999) and Dinar (Wright *et al.*, 1999).

4.6.4 Related Phenomena

INSAR and CGPS open two new windows in the spatio-temporal spectrum of seismological metrology: INSAR at distance scales between ~ 1 and ~ 10 km; CGPS at timescales of days to years. Prior to the introduction of these two techniques, measurements at these scales were prohibitively expensive or prone to drift. Now that both techniques have entered the realm of operational, routine observations, we should expect to see interesting observations of other seismological phenomena, such as slow earthquakes, interseismic strain accumulation, and perhaps even an earthquake precursor.

Acknowledgments

I thank Alexis Rigo, Jean-Claude Ruegg and Didier Massonnet for helpful discussions. Partially financed by l'Institut National des Sciences de l'Univers and GDR INSAR.

References

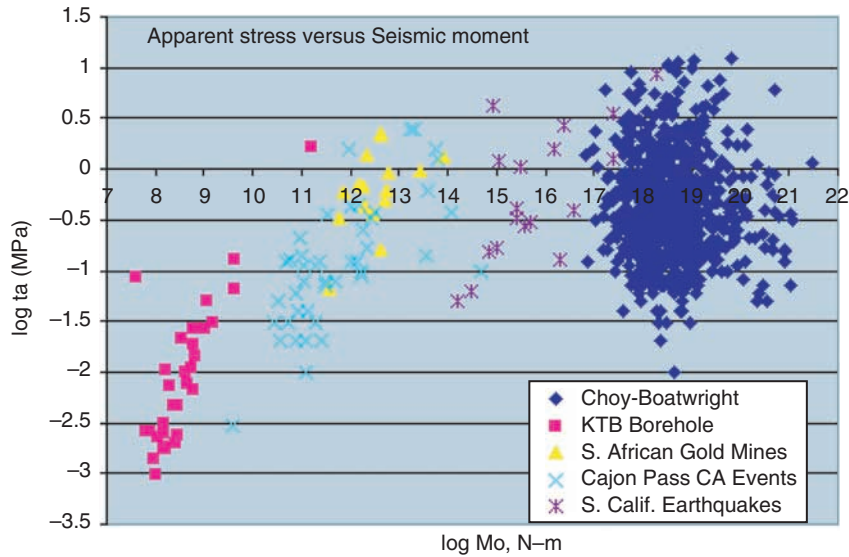
- Abe, K. (1995). In: "Global Earth Physics: a Handbook of Physical Constants," vol. 1, pp. 206–213, American Geophysics Union.
- Aki, K. and P.G. Richards (1980). "Quantitative Seismology," Freeman.
- Arnadottir, T. and P. Segall (1994). *J. Geophys. Res.* **99**, 21835–21856.
- Arnadottir, T., *et al.* (1991). *Geophys. Res. Lett.* **18**, 2217–2220.
- Arnadottir, T., *et al.* (1992). *Bull. Seismol. Soc. Am.* **82**, 2248–2255.
- Arnadottir, T., *et al.* (1995). *NZ J. Geol. Geophys.* **38**, 553–558.
- Bamler, R. and P. Hartl (1998). *Inverse Probl.* **14**, R1–R54.
- Barrientos, S.E. and S.N. Ward (1990). *Geophys. J. Int.* **103**, 589–598.
- Barrientos, S.E., *et al.* (1987). *Bull. Seismol. Soc. Am.* **77**, 784–808.
- Beauducel, F., *et al.* (2000). *J. Geophys. Res.* **104**, 16391–.
- Bennett, R.A., *et al.* (1994). *J. Geophys. Res.* **100**, 6443–6461.
- Bernard, P., *et al.* (1997). *J. Seismol.* **1**, 131–150.
- Bezzeghoud, M., *et al.* (1995). *Tectonophysics* **249**, 249–266.
- Bilham, R. (1991). *Rev. Geophys.* **29**, 1–30.
- Bilham, R. (1998). *Appalachia* **47**, **187**, 79–107.
- Bock, Y., *et al.* (1993). *Nature* **361**, 337–340.
- Bock, Y., *et al.* (1997). *J. Geophys. Res.* **102**, 18013–18033.
- Bomford, G. (1980). "Geodesy," 4th Edn. Oxford University Press.
- Bürgmann, R., *et al.* (1997). *J. Geophys. Res.* **102**, 4933–4955.
- Calais, E., *et al.* (1993). *C. R. Acad. Sci. Paris* **317 II**, 1493–1500.
- Cattin, R., *et al.* (1999). *Geophys. J. Int.* **137**, 149–158.
- Chen, J., *et al.* (1984). In: "The International Karakoram Project," Cambridge University Press.
- Clark, T.A., *et al.* (1990). *Geophys. Res. Lett.* **17**, 1215–1218.
- Clarke, P.J., *et al.* (1996). *Geophys. Res. Lett.* **24**, 707–710.
- Clarke, P.J., *et al.* (1998). *Geophys. Res. Lett.* **25**, 131–134.
- Cohee, B.P. and G.C. Beroza (1994). *Bull. Seismol. Soc. Am.* **84**, 692–712.
- Cotton, F. and M. Campillo (1994). *J. Geophys. Res.* **100**, 3961–3975.
- Cotton, F. and M. Campillo (1995). *Geophys. Res. Lett.* **22**, 1921–1924.
- Crétaux, J.-F., *et al.* (1998). *J. Geophys. Res.* **103**, 30167–30182.
- Crippen, R.E. (1992). *Episodes* **15**, 56–61.
- Crippen, R.E. and R.G. Blom (1992). *Trans. Am. Geophys. Un.* **73**, 364.
- Crook, C.N., *et al.* (1982). *US Geol. Surv. Prof. Paper* **1254**, 183–191.
- Cummins, P.R., *et al.* (1998). *Geophys. Res. Lett.* **25**, 3219–3222.
- Curlander, J.C., *et al.* (1991). "Synthetic Aperture Radar: Systems and Signal Processing," Wiley.
- Dal Moro, G. and M. Zadro (1999). *Earth Planet. Sci. Lett.* **170**, 119–129.
- Delacourt, C., *et al.* (1998). *Geophys. Res. Lett.* **25**, 2849–2852.
- Dixon, T.H. (1991). *Rev. Geophys.* **29**, 249–276.
- DMA (1987). *DMA TR 8350.2-B*, Defense Mapping Agency.
- Dolan, J.F., *et al.* (1995). *Science* **267**, 199–205.
- Du, Y.J., *et al.* (1994). *J. Geophys. Res.* **99**, 3767–3779.
- Duquesnoy, T., *et al.* (1996). *Geophys. Res. Lett.* **23**, 3055–3058.
- Dvorak, J. (1994). *J. Geophys. Res.* **99**, 9533–9542.
- Dziewonski, A.M. and D.L. Anderson (1981). *Phys. Earth Planet. Inter.* **25**, 297–356.
- Eberhardt-Phillips, D. (1989). *J. Geophys. Res.* **94**, 15565–15586.
- Ekstrom, G., *et al.* (1992). *J. Geophys. Res.* **97**, 4843–4864.

- Feigl, K.L. and E. Dupré (1999). *Comput. Geosci.* **25**, 695–704.
- Feigl, K.L., *et al.* (1995). *Geophys. Res. Lett.* **22**, 1037–1048.
- Feigl, K.L., *et al.* (2000). *J. Geophys. Res.* **105**, 25655–.
- Frey Mueller, J., *et al.* (1994). *Bull. Seismol. Soc. Am.* **84**, 646–659.
- Ghiglia, D.C. (1998). “Two-dimensional Phase Unwrapping: Theory, Algorithms, and Software,” Wiley.
- Goldstein, R. (1995). *Geophys. Res. Lett.* **22**, 2517–2520.
- Hager, B.H., *et al.* (1991). *Annu. Rev. Earth Planet. Sci.* **19**, 351–382.
- Hanks, T.C. and H. Kanamori (1979). *J. Geophys. Res.* **84**, 2348–2350.
- Hanssen, R. (1998). “Atmospheric Heterogeneities in ERS Tandem SAR Interferometry,” Delft University Press.
- Harris, R.A. and R.W. Simpson (1992). *Nature* **360**, 251–254.
- Harsh, P.W. (1982). *US Geol. Surv. Prof. Paper 1254*, 193–203.
- Hartzell, S.H. and T.H. Heaton (1983). *Calif. Div. Mines Geol. Spec. Publ.* **66**, 241–246.
- Henderson, F.M. and A.J. Lewis (Eds.) (1998). “Principles and Applications of Imaging Radar,” Wiley.
- Hernandez, B., *et al.* (1997). *Geophys. Res. Lett.* **24**, 1579–1582.
- Hernandez, B., *et al.* (1999). *J. Geophys. Res.* **104**, 13083–13099.
- Herring, T.A. (1992). *J. Geophys. Res.* **97**, 1981–1990.
- Holdahl, S.R. and J. Sauber (1994). *Pageoph* **142**, 55–82.
- Huang, B.S. and Y.T. Yeh (1997). *Bull. Seismol. Soc. Am.* **87**, 1046–1057.
- Hudnut, K.W. (1995). *Rev. of Geophys. Suppl.* 249–255.
- Hudnut, K.W., *et al.* (1994). *Bull. Seismol. Soc. Am.* **84**, 625–645.
- Hudnut, K.W., *et al.* (1995). *Bull. Seismol. Soc. Am.* **86**, S49–S70.
- Ihmlé, P. and J.-C. Ruegg (1997). *Geophys. J. Int.* **131**, 146–158.
- Jaumé, S.C. and L.R. Sykes (1992). *Science* **258**, 1325–1328.
- Johnson, H.O., *et al.* (1994). *Bull. Seismol. Soc. Am.* **84**, 660–667.
- Kanamori, H. (1973). *Annu. Rev. Earth Planet. Sci.* **1**, 212–239.
- Klotz, J., *et al.* (1999). *Pageoph* **194**, in press.
- Larsen, S., *et al.* (1992). *J. Geophys. Res.* **97**, 4885–4902.
- Larson, K.M. (1995). *Rev. Geophys. Suppl.* 371–377.
- Lefebvre, M., *et al.* (1996). *EOS* **77**, 25–29.
- Lépine, J.C., *et al.* (1979). *Bull. Soc. Geol. Fr.* **22**, 817–822.
- Lin, J. and R.S. Stein (1989). *J. Geophys. Res.* **94**, 9614–9632.
- Lisowski, M., *et al.* (1990). *Geophys. Res. Lett.* **17**, 1437–1440.
- Lundgren, P.R., *et al.* (1993). *Geophys. Res. Lett.* **20**, 407–410.
- Madsen, S.N. and H.A. Zebker (1998). *Manual of Remote Sensing* **2**, 359–380.
- Marshall, G.A., *et al.* (1991). *Bull. Seismol. Soc. Am.* **81**, 1660–1693.
- Massonnet, D. and K.L. Feigl (1995a). *Geophys. Res. Lett.* **22**, 1537–1540.
- Massonnet, D. and K.L. Feigl (1995b). *Geophys. Res. Lett.* **22**, 1541–1544.
- Massonnet, D. and K.L. Feigl (1998). *Rev. Geophys.* **36**, 441–500.
- Massonnet, D. and T. Rabaute (1993). *IEEE Trans. Geosci. Remote Sens.* **31**, 455–464.
- Massonnet, D., *et al.* (1994). *Nature* **369**, 227–230.
- Massonnet, D., *et al.* (1996a). *Geophys. Res. Lett.* **23**, 969–972.
- Massonnet, D., *et al.* (1996b). *Nature* **382**, 612–616.
- Matthews, M.V. and P. Segall (1993). *J. Geophys. Res.* **98**, 12153–12163.
- Meade, B.K. and R.W. Miller (1973). In: “San Fernando, California, Earthquake of February 9, 1971,” Vol. III, pp. 243–293. NOAA.
- Melbourne, T., *et al.* (1997). *Geophys. Res. Lett.* **24**, 715–718.
- Meyer, B., *et al.* (1996). *Geophys. Res. Lett.* **23**, 2677–2680.
- Meyer, B., *et al.* (1998). *Geophys. Res. Lett.* **25**, 129–130.
- Michel, R., *et al.* (1999). *Geophys. Res. Lett.* **26**, 875–878.
- Milbert, D.G. and W.T. Dewhurst (1992). *J. Geophys. Res.* **97**, 545–557.
- Miyazaki, S., *et al.* (1996). *Bull. Geogr. Surv. Inst. (Japan)* **42**, 27–41.
- Morrison, N.L. (1973). In: “San Fernando, California, Earthquake of February 9, 1971,” Vol. III, pp. 295–324. NOAA.
- Murakami, M., *et al.* (1996). *J. Geophys. Res.* **101**, 8605–8614.
- Murray, M.H., *et al.* (1996). *J. Geophys. Res.* **101**, 17707–17725.
- Murray, M.H., *et al.* (1993). *Geophys. Res. Lett.* **20**, 623–626.
- Noomen, R., *et al.* (1996). *J. Geodynam.* **21**, 73–96.
- Okada, Y. (1985). *Bull. Seismol. Soc. Am.* **75**, 1135–1154.
- Okada, Y. (1992). *Bull. Seismol. Soc. Am.* **82**, 1018–1040.
- Ozawa, S., *et al.* (1997). *Geophys. Res. Lett.* **24**, 2327–2330.
- Peltzer, G. and P. Rosen (1995). *Science* **268**, 1333–1336.
- Peltzer, G., *et al.* (1996). *Science* **273**, 1202–1204.
- Peltzer, G., *et al.* (1998). *J. Geophys. Res.* **103**, 30131–30146.
- Perrier, G. and J.C. Ruegg (1973). *Ann. Geophys.* **29**, 435–502.
- Pollitz, F., *et al.* (2000). *J. Geophys. Res.* **105**, 8035–8054.
- Pollitz, F.F. (1996). *Geophys. J. Int.* **125**, 1–14.
- Prescott, W.H., *et al.* (1979). *J. Geophys. Res.* **84**, 5423–5435.
- Price, E.J. and D.T. Sandwell (1998). *J. Geophys. Res.* **103**, 27001–27016.
- Reilinger, R.E., *et al.* (2000). *Science in press*.
- Rigo, A. and D. Massonnet (1999). *Geophys. Res. Lett.* **26**, 3217–3220.
- Rosen, P.A., *et al.* (1996). *J. Geophys. Res.* **101**, 23109–23125.
- Ruegg, J.C., *et al.* (1979). *Geophys. Res. Lett.* **6**, 817–820.
- Ruegg, J.C., *et al.* (1982). *Bull. Seismol. Soc. Am.* **72**, 2227–2244.
- Ruegg, J.C., *et al.* (1996). *Geophys. Res. Lett.* **23**, 917–920.
- Sandwell, D.T., *et al.* (2000). *Geophys. Res. Lett.* **in press**.
- Satake, K. (1993). *J. Geophys. Res.* **98**, 4553–4565.
- Sauber, J.M., *et al.* (1993). In: “Contributions of Space Geodesy to Geodynamics: Crustal Dynamics,” Vol. 23, pp. 233–248, American Geophysics Union.
- Savage, J.C. and R.O. Burford (1970). *Bull. Seismol. Soc. Am.* **60**, 1877–1896.
- Savage, J.C. and J.L. Svarc (1997). *J. Geophys. Res.* **102**, 7565–7577.
- Savage, J.C., *et al.* (1993). *J. Geophys. Res.* **98**, 19951–19958.
- Savage, J.C., *et al.* (1994). *J. Geophys. Res.* **99**, 13757–13765.
- Scholz, C.H. (1990). “Earthquakes and Fault Mechanics,” Cambridge University Press.
- Segall, P. and J.L. Davis (1997). *Annu. Rev. Earth. Planet. Sci.* **25**, 301–336.
- Segall, P. and Y. Du (1993). *J. Geophys. Res.* **98**, 4527–4538.
- Shen, Z., *et al.* (1994). *Bull. Seismol. Soc. Am.* **84**, 780–791.
- Shen, Z.K., *et al.* (1996). *Bull. Seismol. Soc. Am.* **86**, S37–S48.
- Sillard, P., *et al.* (1998). *Geophys. Res. Lett.* **25**, 3223–3226.
- Smith, D.E. and D.L. Turcotte (Eds.) (1993). “Contributions of Space Geodesy to Geodynamics: Crustal Dynamics,” American Geophysics Union.
- Smith, D.E., *et al.* (1994). *Geophys. Res. Lett.* **21**, 1979–1982.
- Stein, R.S. and S.E. Barrientos (1985). *J. Geophys. Res.* **90**, 11355–11366.
- Stein, R.S. and G.C.P. King (1984). *Science* **224**, 869–872.
- Stein, R.S., *et al.* (1991). *J. Geophys. Res.* **96**, 21789–21806.
- Stein, R.S., *et al.* (1992). *Science* **258**, 1328–1332.
- Stein, R.S., *et al.* (1994). *Science* **265**, 1432–1435.

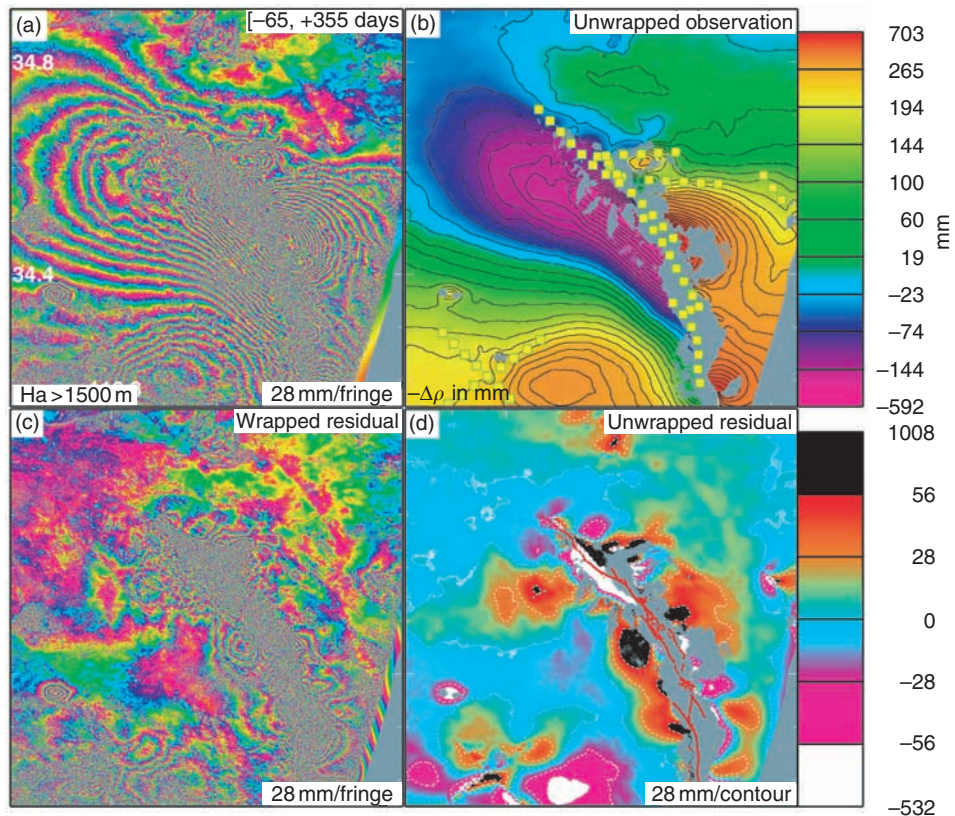
- Stiros, S.C. and A. Drakos (2000). *Geophys. J. Int.* **in press**.
- Tabei, T., *et al.* (1996). *J. Phys. Earth* **in press**.
- Tapley, B.D., *et al.* (1993). In: "Contributions of Space Geodesy to Geodynamics: Earth Dynamics," Vol. 24, pp. 147–173, American Geophysics Union.
- Tarayre, H. (1994). PhD thesis, U. P. Sabatier, Toulouse.
- Tarayre, H. and D. Massonnet (1996). *Geophys. Res. Lett.* **23**, 989–992.
- Thatcher, W. (1974). *Science* **184**, 1283–1285.
- Thatcher, W., *et al.* (1997). *J. Geophys. Res.* **102**, 5353–5367.
- Thio, H.K. and H. Kanamori (1996). *Bull. Seismol. Soc. Am.* **86**, S84–S92.
- Trouvé, E. (1996). PhD thesis, Ecole Nat. Sup. Telecommunications, Paris.
- Trouvé, E., *et al.* (1998). *IEEE Trans. Geosci. Remote Sen.* **36**, 1963–1972.
- Tsuji, H., *et al.* (1995). *Geophys. Res. Lett.* **22**, 1669–1672.
- Vincent, F. (1998). DEA thesis, U. Nice, Sophia-Antipolis, France.
- Wald, D.J. and T.H. Heaton (1994). *Bull. Seismol. Soc. Am.* **84**, 668–691.
- Wald, D.J., *et al.* (1996). *Bull. Seismol. Soc. Am.* **86**, S49–S70.
- Ward, S. and S. Barrientos (1986). *J. Geophys. Res.* **91**, 4909–4919.
- Williams, C.R., *et al.* (1993). *J. Geophys. Res.* **98**, 4567–4578.
- Williams, S., *et al.* (1998). *J. Geophys. Res.* **103**, 27051–27068.
- Wolf, M. and D. Wingham (1992). *Geophys. Res. Lett.* **19**, 2325–2328.
- Wright, T.J., *et al.* (1999). *Earth Planet. Sci. Lett.* **172**, 23–27.
- Wyatt, F.K. (1988). *J. Geophys. Res.* **93**, 7923–7942.
- Wyatt, F.K., *et al.* (1994). *Bull. Seismol. Soc. Am.* **84**, 768–779.
- Zebker, H. and R. Goldstein (1986). *J. Geophys. Res.* **91**, 4993–5001.
- Zebker, H.A., *et al.* (1994). *J. Geophys. Res.* **99**, 19617–19634.
- Zebker, H.A., *et al.* (1997). *J. Geophys. Res.* **102**, 7547–7563.
- Zumberge, J.F., *et al.* (1996). International GPS Service 1995 Annual report, IGS Central Bureau, Pasadena.

Editor's Note

Due to space limitations, references with full citation are given in the Handbook CD-ROM under directory \37Feigl as a Microsoft Word file: FeiglFullReferences.doc. An equivalent PDF file is also provided on the CD. Please see also Chapter 35, Strength and energetics of active fault zones, by Brune and Thatcher; and Chapter 36, Implications of crustal strain during conventional, slow and silent earthquakes, by Johnston and Linde.



Color Plate 13 Apparent stress versus seismic moment (M_0). Data sources: KTB borehole events, Zoback and Hartjes (1997); South African mine tremors, McGarr, 1999; Cajon Pass, Abercrombie (1995); Southern California, Kanamori *et al.* (1993). Modified from McGarr (1999).



Color Plate 14 Coseismic deformation field for the Landers earthquake measured by INSAR. (a) Observed “wrapped” interferogram, shown as 28-mm fringes. (b) Observed “unwrapped” interferogram in mm (Trouvé, 1996; Trouvé *et al.*, 1998). (c) Residual (observed minus calculated) wrapped interferogram, shown as 28-mm fringes. (d) Residual unwrapped interferogram in mm. The interferogram is calculated from ERS-1 SAR images taken before (April 24, 1992) and after (June 18, 1993) the earthquake (Massonnet *et al.*, 1994). Each fringe in parts a and c denotes 28 mm of change in range. Here, the altitude of ambiguity h_a exceeds 1500 m.

Chapter 37. Estimating Earthquake Source Parameters from Geodetic Measurements: Full References

Kurt L. Feigl, Centre National de la Recherche Scientifique, Toulouse, France

- Abe, K. (1995). Moments and magnitudes of earthquakes. *In "Global earth physics : a handbook of physical constants"* (J. Ahrens, Ed.), Vol. 1, pp. 206-213. American Geophysical Union, Washington, DC.
- Aki, K., and Richards, P. G. (1980). "Quantitative Seismology", W. H. Freeman, San Francisco.
- Arnadottir, T., Beavan, J., and Pearson, C. (1995). Deformation associated with the 18 June, 1994, Arthur's Pass earthquake, New Zealand, *NZ J. Geol. Geophys.*, **38**, 553-558.
- Arnadottir, T., and Segall, P. (1994). The 1989 Loma Prieta earthquake imaged from inversion of geodetic data, *J. Geophys. Res.*, **99**, 21,835-21,856.
- Arnadottir, T., Segall, P., and Delaney, P. (1991). A fault model for the 1989 Kilauea south flank earthquake from levelling and seismic data, *Geophys. Res. Lett.*, **18**, 2217-2220.
- Arnadottir, T., Segall, P., and Mathews, M. (1992). Resolving the discrepancy between geodetic and seismic fault models for the 1989 Loma Prieta, California, earthquake, *Bull. Seism. Soc. Amer.*, **82**, 2248-2255.
- Bamler, R., and Hartl, P. (1998). Synthetic aperture radar interferometry, *Inverse Problems*, **14**, R1-R54.
- Barrientos, S. E., Stein, R. S., and Ward, S. N. (1987). A comparison of the 1959 Hebgen Lake, Montana, and 1983 Borah Peak, Idaho, earthquakes from geodetic data, *Bull. Seism. Soc. Am.*, **77**, 784-808.
- Barrientos, S. E., and Ward, S. N. (1990). The 1960 Chile earthquake: inversion for slip distribution from surface deformation, *Geophys. J. Int.*, **103**, 589-598.
- Beauducel, F., Briole, P., and Froger, J. L. (1999). Volcano wide fringes in ERS SAR interferograms of Etna: Deformation or tropospheric effect?, *J. Geophys. Res.*, **in press**,
- Beavan, J. et al., Determination of the Philippine Sea Plate Velocity from Global Positioning System Observations, and Effects of the 1993 Guam Earthquake (abstract), *EOS supplement*, June 21, 59, 1994.
- Bennett, R. A., Reilinger, R. E., Rodi, W., Li, Y., Toksöz, M. N., and Hudnut, K. (1994). Coseismic fault slip associated with the 1992 Mw 6.1 Joshua Tree, California earthquake: implications for the Joshua Tree-Landers earthquake sequence, *J. Geophys. Res.*, **100**, 6443-6461.
- Bernard, P. et al. (1997). The Ms=6.2 June 15, 1995 Aigion earthquake (Greece): results of a multidisciplinary study, *J. Seismol.*, **1**, 131-150.
- Bezzeghoud, M., Dimitrov, D., Ruegg, J. C., and Lammali, K. (1995). Faulting mechanism of the El Asnam (Algeria) 1954 and 1980 earthquakes from modelling of vertical movements, *Tectonophysics*, **249**, 249-266.

- Bilham, R. (1991). Earthquakes and sea level: space and terrestrial metrology on a changing planet, *Rev. Geophys.*, **29**, 1-30.
- Bilham, R. (1998). Mountain metrology and space geodesy, *Appalachia*, **47**, **187**, 79-107.
- Bock, Y. et al. (1993). Detection of crustal deformation from the Landers Earthquake using continuous geodetic measurements, *Nature*, **361**, 337-340.
- Bock, Y. et al. (1997). Southern California Permanent GPS Geodetic Array: Continuous measurements of regional crustal deformation between the 1992 Landers and 1994 Northridge earthquakes, *J. Geophys. Res.*, **102**, 18013-18033.
- Bomford, G. (1980). "Geodesy", 4th ed. ed.. Oxford University Press, Oxford.
- Bürgmann, R., Segall, P., Lisowski, M., and Svarc, J. (1997). Postseismic strain following the 1989 Loma Prieta earthquake from repeated GPS and leveling measurements, *J. Geophys. Res.*, **102**, 4933-4955.
- Calais, E., Carrier, A., and Buffet, G. (1993). Comparaison of levelling and Global Positioning System data: application to the determination of the geoid in the Alpes-Maritimes, *C. R. Acad. Sci. Paris*, **317 II**, 1493-1500.
- Cattin, R., Briole, P., Lyon-Caen, H., Bernard, P., and Pinettes, P. (1999). Effects of superficial layers on coseismic displacements for a dip-slip fault and geophysical implications, *Geophys. J. Int.*, **137**, 149-158.
- Chen, J., Crompton, T. D., Walton, J. L. W., and Bilham, R. (1984). The survey work of the International Karakoram Project. In "The International Karakoram Project" (K. J. Miller, Ed.), Vol. Cambridge University Press, Cambridge.
- Clark, T. A., Ma, C., Sauber, J. M., Ryan, J. W., Gordon, D., Shaffer, D. B., Chaprette, D. S., and Vandenberg, N. R. (1990). Geodetic measurement of deformation in the Loma Prieta, California earthquake with very long baseline interferometry, *Geophys. Res. Lett.*, **17**, 1215-1218.
- Clarke, P. J., Paradissis, D., Briole, P., England, P. C., Parsons, B. E., Billiris, H., Veis, G., and Ruegg, J.-C. (1996). Geodetic investigation of the 13 May 1995 Kozani-Grevena (Greece) earthquake, *Geophys. Res. Lett.*, **24**, 707-710.
- Clarke, P. J., Paradissis, D., Briole, P., England, P. C., Parsons, B. E., Billiris, H., Veis, G., and Ruegg, J.-C. (1998). Reply to Comment by Meyer et al. on "Geodetic investigation of the May 13, 1995 Kozani-Grevena (Greece) earthquake" by P. J. Clarke et al., *Geophys. Res. Lett.*, **25**, 131-134.
- Cohee, B. P., and Beroza, G. C. (1994). Slip distribution of the 1992 Landers earthquake and its implications for earthquake source mechanics, *Bull. Seism. Soc. Am.*, **84**, 692-712.
- Cotton, F., and Campillo, M. (1994). Frequency domain inversion of strong motions: application to the 1992 Landers earthquakes, *J. Geophys. Res.*, **100**, 3961-3975.
- Cotton, F., and Campillo, M. (1995). Stability of the rake during the 1992 Landers earthquake. An indication for a small stress release?, *Geophys. Res. Lett.*, **22**, 1921-1924.
- Crétau, J.-F., Soudarin, L., Cazenave, A., and Bouillé, F. (1998). Present-day tectonic plate motions and crustal deformations from the DORIS space system, *J. Geophys. Res.*, **103**, 30,167-30,182.
- Crippen, R. E. (1992). Measurement of subresolution terrain displacements using SPOT panchromatic imagery, *Episodes*, **15**, 56-61.

- Crippen, R. E., and Blom, R. G., The first visual observation of fault movements from space: the 1992 Landers Earthquake (abstract), *Trans. Amer. Geophys. Un.*, **73**, 364, 1992.
- Crook, C. N., Mason, R. G., and Wood, P. R. (1982). Geodetic measurements of horizontal deformation on the Imperial Fault. In "The Imperial Valley, California earthquake of October 15, 1979. Geological Survey Professional Paper 1254" (U.S. Geological Survey, Ed.), Vol. pp. 183-191. U.S. Gov't Printing Office, Washington, D.C.
- Cummins, P. R., Hirano, S., and Kaneda, Y. (1998). Refined coseismic displacement modeling for the 1994 Shikotan and Sanriku-oki earthquakes, *Geophys. Res. Lett.*, **25**, 3219-3222.
- Curlander, J. C., and McDonough, R. N. (1991). "Synthetic Aperture Radar: Systems and Signal Processing", Wiley, New York.
- Dal Moro, G., and Zadro, M. (1999). Remarkable tilt-strain anomalies preceding two seismic events in Friuli (NE Italy): their interpretation as precursors, *Earth Planet. Sci. Lett.*, **170**, 119-129.
- Delacourt, C., Briole, P., and Achache, J. (1998). Tropospheric corrections of SAR interferograms with strong topography. Application to Etna, *Geophys. Res. Lett.*, **25**, 2849-2852.
- Dixon, T. H. (1991). An introduction to the Global Positioning System and some geological applications, *Rev. Geophys.*, **29**, 249-276.
- DMA (1987). Supplement to Department of Defense World Geodetic System 1984 Technical Report: Part II -- Parameters, Formulas and Graphics for the Practical Application of WGS84, *DMA TR 8350.2-B*, Defense Mapping Agency.
- Dolan, J. F., Sieh, K., Rockwell, T. K., Yeats, R. S., Shaw, J., Suppe, J., Huftile, G. J., and Gath, E. M. (1995). Prospects for larger or more frequent earthquakes in the Los Angeles metropolitan region, *Science*, **267**, 199-205.
- Du, Y. J., Segall, P., and Gao, H. J. (1994). Dislocations in inhomogeneous media via a moduli perturbation approach: general formulation and two-dimensional solutions, *J. Geophys. Res.*, **99**, 3767-3779.
- Duquesnoy, T., Bellier, O., Kasser, M., Sebrier, M., Vigny, C., and Bhaar, I. (1996). Deformation related to the 1994 Liwa earthquake derived from geodetic measurements, *Geophys. Res. Lett.*, **23**, 3055-3058.
- Dvorak, J. (1994). An earthquake cycle along the south flank of Kilauea Volcano, Hawaii, *J. Geophys. Res.*, **99**, 9533-9542.
- Dziewonski, A. M., and Anderson, D. L. (1981). Preliminary reference Earth model, *Phys. Earth Plan. Int.*, **25**, 297-356.
- Eberhardt-Phillips, D. (1989). Active Faulting and Deformation of the Coalinga Anticline as Interpreted From 3-Dimensional Velocity Structure and Seismicity, *J. Geophys. Res.*, **94**, 15565-15586.
- Ekstrom, G., Stein, R. S., Eaton, J. P., and Eberhardt-Phillips, D. (1992). Seismicity and geometry of a 110-km-long blind thrust fault, 1, the 1985 Kettleman Hills, California earthquake, *J. Geophys. Res.*, **97**, 4843-4864.
- Feigl, K. L., and Dupré, E. (1999). RINGCHN: a program to calculate displacement components from dislocations in an elastic half-space with applications for modeling geodetic measurements of crustal deformation, *Computers and Geosciences*, **25**, 695-704.

- Feigl, K. L., Gasperi, J., Sigmundsson, F., and Rigo, A. (1999). Crustal deformation near Hengill volcano, Iceland 1993-1998: coupling between volcanism and faulting inferred from elastic modeling of satellite radar interferograms, *J. Geophys. Res.*, **in press**,
- Feigl, K. L., Sargent, A., and Jacq, D. (1995). Estimation of an earthquake focal mechanism from a satellite radar interferogram: application to the December 4, 1992 Landers aftershock, *Geophys. Res. Lett.*, **22**, 1037-1048.
- Frey Mueller, J., King, N. E., and Segall, P. (1994). The coseismic slip distribution of the Landers earthquake, *Bull. Seism. Soc. Am.*, **84**, 646-659.
- Ghiglia, D. C. (1998). "Two-dimensional phase unwrapping: theory, algorithms, and software", Wiley, New York.
- Goldstein, R. (1995). Atmospheric limitations to repeat-track radar interferometry, *Geophys. Res. Lett.*, **22**, 2517-2520.
- Hager, B. H., King, R. W., and Murray, M. H. (1991). Measurement of crustal deformation using the Global Positioning System, *Ann. Rev. Earth Planet. Sci.*, **19**, 351-82.
- Hanks, T. C., and Kanamori, H. (1979). A moment magnitude scale, *J. Geophys. Res.*, **84**, 2348-2350.
- Hanssen, R. (1998). "Atmospheric heterogeneities in ERS tandem SAR interferometry", Delft University Press, Delft, Netherlands.
- Harris, R. A., and Simpson, R. W. (1992). Changes in static stress on southern California faults after the 1992 Landers earthquake, *Nature*, **360**, 251-254.
- Harsh, P. W. (1982). Distribution of afterslip along the Imperial Fault. In "The Imperial Valley, California earthquake of October 15, 1979. Geological Survey Professional Paper 1254" (U.S. Geological Survey, Ed.), Vol. pp. 193-203. U.S. Gov't Printing Office, Washington, D.C.
- Hartzell, S. H., and Heaton, T. H. (1983). Teleseismic mechanism of the May 2, 1983, Coalinga California earthquake from long-period P waves. In "The 1983 Coalinga Earthquakes" (J. H. Bennett, and R. W. Sherburne, Ed.), Vol. 66, pp. 241-246. Calif. Div. Mines and Geol. Spec. Publ.,
- Henderson, F. M., and Lewis, A. J. (ed.) (1998). "Principles and applications of Imaging Radar", 3rd ed.. Wiley, New York.
- Hernandez, B., Cotton, F., and Campillo, M. (1999). Contribution of radar interferometry to a two step inversion of the kinematic process of the 1992 Landers earthquake, *J. Geophys. Res.*, **in press**,
- Hernandez, B., Cotton, F., Campillo, M., and Massonnet, D. (1997). A comparison between short-term (co-seismic) and long-term (one year) slip for the Landers earthquake: Measurements from strong motion and SAR interferometry, *Geophys. Res. Lett.*, **24**, 1579-1582.
- Herring, T. A. (1992). Submillimeter horizontal position determination using Very Long Baseline Interferometry, *J. Geophys. Res.*, **97**, 1981-1990.
- Holdahl, S. R., and Sauber, J. (1994). Coseismic slip in the 1964 Prince William Sound earthquake: a new geodetic inversion, *Pageoph*, **142**, 55-82.
- Huang, B. S., and Yeh, Y. T. (1997). The fault ruptures of the 1976 Tangshan earthquake sequence inferred from coseismic crustal deformation, *Bull. Seism. Soc. Amer.*, **87**, 1046-1057.

- Hudnut, K. W. (1995). Earthquake geodesy and hazard monitoring, *Reviews of Geophysics (Supplement: U. S. National Report to IUGG, 1991-1994)*, 249-255.
- Hudnut, K. W. et al. (1994). Coseismic displacements of the 1992 Landers earthquake sequence, *Bull. Seism. Soc. Amer.*, **84**, 625–645.
- Hudnut, K. W. et al. (1995). Co-seismic displacements of the 1994 Northridge, California earthquake, *Bull. Seism. Soc. Amer.*, **86**, S49-S70.
- Ihmlé, P., and Ruegg, J.-C. (1997). Source tomography by simulated annealing using broad-band surface waves and geodetic data: application to the Mw = 8.1 Chile 1995 event, *Geophys. J. Int.*, **131**, 146-158.
- Jaumé, S. C., and Sykes, L. R. (1992). Changes in state of stress on the southern San Andreas fault resulting from the California earthquake sequence of April to June, 1992, *Science*, **258**, 1325-1328.
- Johnson, H. O., Agnew, D. C., and Hudnut, K. (1994). Extremal bounds on earthquake moment from geodetic data: application to the Landers earthquake, *Bull. Seism. Soc. Amer.*, **84**, 660–667.
- Kanamori, H. (1973). Mode of strain release associated with major earthquakes in Japan, *Ann. Rev. Earth Plan. Sci.*, **1**, 212-239.
- Klotz, J. et al. (1999). GPS-derived deformation of the Central Andes including the 1995 Antofagasta Mw = 8.0 earthquake, *PAGEOPH*, **194**, in press.
- Larsen, S., Reilinger, R., Neugebauer, H., and Strange, W. (1992). Global Positioning System Measurements of deformations associated with the 1987 Superstition Hills earthquake: evidence for conjugate faulting, *J. Geophys. Res.*, **97**, 4885-4902.
- Larson, K. M. (1995). Crustal Deformation, *U.S. National Report to International Union of Geodesy and Geophysics 1991-1994, Reviews of Geophysics Supplement*, 371-377.
- Lefebvre, M., Cazenave, A., Escudier, P., Biancale, R., Cretaux, J. F., Soudarin, L., and Valette, J. J. (1996). Space tracking system improves accuracy of geodetic measurements, *Eos*, **77**, 25-29.
- Lépine, J. C., Ruegg, J.-C., and Abdallah, A. M. (1979). Sismicité du rift d'Asal-Ghoubbet pendant la crise sismo-volcanique de novembre 1978, *Bull. Soc. Geol. Fr.*, **22**, 817-822.
- Lin, J., and Stein, R. S. (1989). Coseismic folding, earthquake recurrence, and the 1987 source mechanism at Whittier Narrows, Los Angeles basin, California, *J. Geophys. Res.*, **94**, 9614-9632.
- Lisowski, M., Prescott, W. H., Savage, J. C., and Johnston, M. L. (1990). Geodetic estimate of coseismic slip during the 1989 Loma Prieta, California, earthquake, *Geophys. Res. Lett.*, **17**, 1437-1440.
- Lundgren, P. R., Wolf, S. K., Protti, M., and Hurst, K. J. (1993). GPS measurements of crustal deformation associated with the 22 April 1991, Valle de la Estrella, Costa Rica earthquake, *Geophys. Res. Lett.*, **20**, 407-410.
- Madsen, S. N., and Zebker, H. A. (1998). Imaging radar interferometry. In "Principles and Applications of Imaging Radar" (F. M. Henderson, and A. J. Lewis, Ed.), *Manual of Remote Sensing*, Vol. 2, pp. 359-380. Wiley, New York.
- Marshall, G. A., Stein, R. S., and Thatcher, W. (1991). Faulting geometry and slip from co-seismic elevation changes: the 18 October 1989, Loma Prieta, California earthquake, *Bull. Seism. Soc. Am.*, **81**, 1660-1693.

- Massonnet, D., and Feigl, K. L. (1995a). Discriminating geophysical phenomena in satellite radar interferograms, *Geophys. Res. Lett.*, **22**, 1537-1540.
- Massonnet, D., and Feigl, K. L. (1995b). Satellite radar interferometric map of the coseismic deformation field of the M = 6.1 Eureka Valley, California earthquake of May 17, 1993, *Geophys. Res. Lett.*, **22**, 1541-1544.
- Massonnet, D., and Feigl, K. L. (1998). Radar interferometry and its application to changes in the Earth's surface, *Rev. Geophys.*, **36**, 441-500.
- Massonnet, D., Feigl, K. L., Rossi, M., and Adragna, F. (1994). Radar interferometric mapping of deformation in the year after the Landers earthquake, *Nature*, **369**, 227-230.
- Massonnet, D., Feigl, K. L., Vadon, H., and Rossi, M. (1996a). Coseismic deformation field of the M = 6.7 Northridge, California earthquake of January 17, 1994 recorded by two radar satellites using interferometry, *Geophys. Res. Lett.*, **23**, 969-972.
- Massonnet, D., and Rabaute, T. (1993). Radar interferometry: limits and potential, *IEEE Trans. Geoscience & Rem. Sensing*, **31**, 455-464.
- Massonnet, D., Thatcher, W., and Vadon, H. (1996b). Detection of postseismic fault zone collapse following the Landers earthquake, *Nature*, **382**, 612-616.
- Matthews, M. V., and Segall, P. (1993). Statistical inversion of crustal deformation data and estimation of the depth distribution of slip in the 1906 earthquake, *J. Geophys. Res.*, **98**, 12,153-12,163.
- Meade, B. K., and Miller, R. W. (1973). Horizontal crustal movements determined from surveys after San Fernando earthquake. In "San Fernando, California, Earthquake of February 9, 1971" (N. A. Benfer, J. L. Coffman, and J. R. Bernick, Ed.), Vol. III, pp. 243-293. National Oceanic and Atmospheric Administration, Washington, D.C.
- Melbourne, T., Carmichael, I., DeMets, C., Hudnut, K., Sanchez, O., Stock, J., Suarez, G., and Webb, F. (1997). The geodetic signature of the M 8.0 October 9, Jalisco subduction earthquake, *Geophys. Res. Lett.*, **24**, 715-718.
- Meyer, B., Armijo, R., Massonnet, D., de Chaballier, J. B., Delacourt, C., Ruegg, J. C., Achache, J., Briole, P., and Panastassiou, D. (1996). The 1995 Grevena (Northern Greece) earthquake: fault model constrained with tectonic observations and SAR interferometry, *Geophys. Res. Lett.*, **23**, 2677-2680.
- Meyer, B., Armijo, R., Massonnet, D., de Chaballier, J. B., Delacourt, C., Ruegg, J. C., Achache, J., and Papanastassiou, D. (1998). Comment on "Geodetic investigation on the May 13, 1995 Kozani-Grevena (Greece) earthquake" by Clarke et al., *Geophys. Res. Lett.*, **25**, 129-130.
- Michel, R., Avouac, J. P., and Taboury, J. (1999). Measuring ground displacements from SAR amplitude images: application to the Landers earthquake, *Geophys. Res. Lett.*, **26**, 875-878.
- Milbert, D. G., and Dewhurst, W. T. (1992). The Yellowstone-Hebgen Lake geoid obtained through the integrated geodesy approach, *J. Geophys. Res.*, **97**, 545-557.
- Miyazaki, S. et al. (1996). Establishment of the nationwide GPS array (GRAPES) and its initial results on the crustal deformation of Japan, *Bull. Geogr. Surv. Inst. (Japan)*, **42**, 27-41.
- Morrison, N. L. (1973). Vertical crustal movements determined from surveys before and after San Fernando earthquake. In "San Fernando, California, Earthquake of February 9, 1971" (N. A. Benfer, J. L. Coffman, and J. R. Bernick, Ed.), Vol. III, pp. 295-324. National Oceanic and Atmospheric Administration, Washington, D.C.

- Murakami, M., Tobita, M., Saito, T., and Masharu, H. (1996). Coseismic crustal deformations of the 1994 Northridge, California earthquake detected by interferometric analysis of SAR images acquired by the JERS-1 satellite, *J. Geophys. Res.*, **101**, 8605-8614.
- Murray, M. H., Marshall, G. A., Lisowski, M., and Stein, R. S. (1996). The 1992 M = 7 Cape Mendocino, California earthquake: Coseismic deformation at the souther end of the Cascadia megathrust, *J. Geophys. Res.*, **101**, 17,707-17,725.
- Murray, M. H., Savage, J. C., Lisowski, M., and Gross, W. K. (1993). Coseismic displacements: 1992 Landers, California Earthquake, *Geophys. Res. Lett.*, **20**, 623-626.
- Noomen, R., Springer, T. A., Ambrosius, B. A. C., Herzerberger, K., Kuijper, D. C., Mets, G.-J., Overgaauw, B., and Wakker, K. F. (1996). Crustal Deformations in the Mediterranean area computed from SLR and GPS observations, *J. Geodynamics*, **21**, 73-96.
- Okada, Y. (1985). Surface deformation to shear and tensile faults in a half-space, *Bull. Seism. Soc. Am.*, **75**, 1135-1154.
- Okada, Y. (1992). Internal deformation due to shear and tensile faults in a half space, *Bull. Seism. Soc. Am.*, **82**, 1018-1040.
- Ozawa, S., Murakami, M., Fujiwara, S., and Tobita, M. (1997). Synthetic aperture radar interferogram of the 1995 Kobe earthquake and its geodetic inversion, *Geophys. Res. Lett.*, **24**, 2327-2330.
- Peltzer, G., and Rosen, P. (1995). Surface displacement of the 17 May 1993 Eureka Valley, California earthquake observed by SAR interferometry, *Science*, **268**, 1333-1336.
- Peltzer, G., Rosen, P., Rogez, F., and Hudnut, K. (1996). Postseismic rebound in fault step-overs caused by pore fluid flow, *Science*, **273**, 1202-1204.
- Peltzer, G., Rosen, P., Rogez, F., and Hudnut, K. (1998). Poroelastic rebound along the Landers 1992 earthquake surface rupture, *J. Geophys. Res.*, **103**, 30,131-30,146.
- Perrier, G., and Ruegg, J. C. (1973). Structure profonde du Massif Central français, *Ann. Geophys.*, **29**, 435-502.
- Pollitz, F., Peltzer, G., and Burgmann, R. (2000). Mobility of continental mantle: evidence from postseismic geodetic observations following the 1992 Landers earthquake, *J. Geophys. Res.*, **105**, 8035-8054.
- Pollitz, F. F. (1996). Coseismic deformation from earthquake faulting on a layered spherical earth, *Geophys. J. Int.*, **125**, 1-14.
- Prescott, W. H., Savage, J. C., and Kinoshita, W. T. (1979). Strain accumulation in the western United States between 1970 and 1978, *J. Geophys. Res.*, **84**, 5423-5435.
- Price, E. J., and Sandwell, D. T. (1998). Small-scale deformations associated with the 1992 Landers, California, earthquake mapped by synthetic aperture radar interferometry phase gradients, *J. Geophys. Res.*, **103**, 27,001-27,016.
- Reilinger, R. E. et al. (2000). Coseismic and postseismic fault slip for the M=7.4, 17 August 1999, Izmit, Turkey earthquake, *Science*, **in press**,
- Rigo, A., and Massonnet, D. (1999). Investigating the 1996 Pyrenean earthquake (France) with SAR Interferograms heavily distorted by atmosphere, *Geophys. Res. Lett.*, **26**, 3217-3220.
- Rosen, P. A., Hensley, S., Zebker, H. A., Webb, F. H., and Fielding, E. J. (1996). Surface deformation and coherence measurements of Kilauea volcano, Hawaii from SIR-C radar interferometry, *J. Geophys. Res.*, **101**, 23,109-23,125.

- Ruegg, J. C. et al. (1996). The Mw = 8.1 Atnofagasta (North Chile) Earthquake of July 30, 1995: First results from geodetic data, *Geophys. Res. Lett.*, **23**, 917-920.
- Ruegg, J. C., Kasser, M., Tarantola, A., Lépine, J. C., and Chouikrat, B. (1982). Deformations associated with the El Asnam earthquake of 10 October 1980: geodetic determination of vertical and horizontal movements, *Bull. Seism. Soc. Amer.*, **72**, 2227-2244.
- Ruegg, J. C., Lépine, J. C., Tarantola, A., and Kasser, M. (1979). Geodetic measurements of rifting associated with a seismo-volcanic crisis in Afar, *Geophys. Res. Lett.*, **6**, 817-820.
- Sandwell, D. T., Sichoix, L., Agnew, D., Bock, Y., and Minster, B. (2000). Near-Real-Time Radar Interferometry of the Mw 7.1 Hector Mine Earthquake, *Geophys. Res. Lett.*, **in press**.
- Satake, K. (1993). Depth distribution of coseismic slip along the Nankai Trough, Japan, from joint inversion of geodetic and tsunami data, *J. Geophys. Res.*, **98**, 4553-4565.
- Sauber, J. M., Clark, T. A., Bell, L. J., Lisowski, M., Ma, C., and Caprette, D. S. (1993). Geodetic measurement of static displacement associated with the 1987-1988 Gulf of Alaska earthquakes. In "Contributions of Space Geodesy to Geodynamics: Crustal Dynamics" (Ed.), Vol. 23, pp. 233-248. Amer. Geophys. Un., Washington.
- Savage, J. C., and Burford, R. O. (1970). Accumulation of tectonic strain in California, *Bull. Seism. Soc. Am.*, **60**, 1877-1896.
- Savage, J. C., Lisowski, M., and Murray, M. (1993). Deformation from 1973 through 1991 in the epicentral area of the 1992, Landers, California earthquake (Ms = 7.5), *J. Geophys. Res.*, **98**, 19,951-19,958.
- Savage, J. C., Lisowski, M., and Svarc, J. L. (1994). Postseismic deformation following the 1989 (M = 7.1) Loma Prieta, California, earthquake, *J. Geophys. Res.*, **99**, 13,757-13,765.
- Savage, J. C., and Svarc, J. L. (1997). Postseismic deformation associated with the 1992 M = 7.5 Landers earthquake, southern California, *J. Geophys. Res.*, **102**, 7565-7577.
- Scholz, C. H. (1990). "Earthquakes and Fault Mechanics", Cambridge University Press, Cambridge.
- Segall, P., and Davis, J. L. (1997). GPS applications for geodynamics and earthquake studies, *Annu. Rev. Earth. Plan. Sci.*, **25**, 301-336.
- Segall, P., and Du, Y. (1993). How similar were the 1934 and 1996 Parkfield earthquakes, *J. Geophys. Res.*, **98**, 4527-4538.
- Shen, Z., Jackson, D., Feng, Y., Kim, M., and Cline, M. (1994). Postseismic deformation following the 1992 Landers earthquake, *Bull. Seism. Soc. Amer.*, **84**, 780-791.
- Shen, Z. K., Ge, B. X., Jackson, D. D., Potter, D., Cline, M., and Sung, L. Y. (1996). Northridge earthquake rupture models based on the Global Positioning System measurements, *Bull. Seism. Soc. Amer.*, **86**, S37-S48.
- Sillard, P., Altamimi, Z., and Boucher, C. (1998). The ITRF96 realization and its associated velocity field, *Geophys. Res. Lett.*, **25**, 3223-3226.
- Smith, D. E., Kolenkewicz, R., Robbins, J. W., Dunn, P. J., and Torrence, M. H. (1994). Horizontal crustal motion in the central and eastern Mediterranean inferred from satellite laser ranging measurements, *Geophys. Res. Lett.*, **21**, 1979-1982.
- Smith, D. E., and Turcotte, D. L. (ed.) (1993). "Contributions of space geodesy to geodynamics: crustal dynamics", American Geophysical Union, Washington.

- Stein, R. S., and Barrientos, S. E. (1985). Planar high-angle faulting in the Basin and Range: geodetic analysis of the 1983 Borah Peak, Idaho, earthquake, *J. Geophys. Res.*, **90**, 11,355-11,366.
- Stein, R. S., Briole, P., Ruegg, J.-C., Tapponnier, P., and Gasse, F. (1991). Contemporary, Holocene, and Quaternary deformation of the Asal rift, Djibouti: Implications for slow-spreading ridges, *J. Geophys. Res.*, **96**, 21,789-21,806.
- Stein, R. S., and King, G. C. P. (1984). Seismic potential revealed by surface folding: 1983 Coalinga, California, earthquake, *Science*, **224**, 869-872.
- Stein, R. S., King, G. C. P., and Lin, J. (1992). Change in failure stress on the southern San Andreas fault system caused by the 1992 magnitude = 7.4 Landers earthquake, *Science*, **258**, 1328-1332.
- Stein, R. S., King, G. C. P., and Lin, J. (1994). Stress triggering of the 1994 M = 6.7 Northridge, California earthquake by its predecessors, *Science*, **265**, 1432-1435.
- Stiros, S. C., and Drakos, A. (2000). Geodetic constraints to the fault pattern of the 1978, Thessaloniki (Northern Greece) earthquake (Ms = 6.4), *Geophys. J. Int.*, **in press**.
- Tabei, T., Kato, T., Catane, J., Chachin, T., Fujimori, K., and al., e. (1996). Crustal deformation associated with the 1995 Hyogen-ken Nanbu earthquake, Japan, derived from GPS measurements, *J. Phys. Earth*, **in press**.
- Tapley, B. D., Schutz, B. E., Eanes, R. J., Ries, J. C., and Watkins, M. M. (1993). Lageos laser ranging contributions to geodynamics, geodesy, and orbital dynamics. In "Contributions of space geodesy to geodynamics: Earth dynamics" (D. E. Smith, and D. L. Turcotte, Ed.), Vol. 24, pp. 147-173. American Geophysical Un., Washington, D.C.
- Tarayre, H. (1994). Extraction de modèles numériques de terrain par interférométrie radar satellitaire: Algorithmie et artefacts atmosphériques, Ph.D. thesis, U. P. Sabatier, Toulouse.
- Tarayre, H., and Massonnet, D. (1996). Atmospheric propagation heterogeneities revealed by ERS-1 interferometry, *Geophys. Res. Lett.*, **23**, 989-992.
- Thatcher, W. (1974). Strain release mechanism of the 1906 San Francisco Earthquake, *Science*, **184**, 1283-1285.
- Thatcher, W., Marshall, G., and Lisowski, M. (1997). Resolution of fault slip along the 470-km-long rupture of the great 1906 San Francisco earthquake, *J. Geophys. Res.*, **102**, 5353-5367.
- Thio, H. K., and Kanamori, H. (1996). Source complexity of the 1994 Northridge earthquake and its relation to aftershock mechanisms, *Bull. Seism. Soc. Amer.*, **86**, S84-S92.
- Trouvé, E. (1996). Imagerie différentielle en radar à ouverture synthétique, Ph. D. thesis, Ecole Nat. Sup. Telecommunications, Paris,
- Trouvé, E., Nicolas, J.-M., and Maître, H. (1998). Improving phase unwrapping techniques by the use of local frequency estimates, *IEEE Transactions on Geoscience and Remote Sensing*, **36**, 1963-1972.
- Tsuji, H., Hatanaka, Y., Sagiya, T., and Hashimoto, M. (1995). Coseismic crustal deformation from the 1994 Hokkaido-Toho-Oki earthquake monitored by a nationwide continuous GPS array in Japan, *Geophys. Res. Lett.*, **22**, 1669-1672.
- Vincent, F. (1998). Apports et limites de l'interférométrie radar pour l'étude des déformations crustales en zone tropicale: application au séisme de Jalisco (Mexique, Mw=8, 09/10/95), DEA thesis, U. Nice, Sophia-Antipolis, France.

- Wald, D. J., and Heaton, T. H. (1994). Spatial and temporal distribution of slip for the 1992 Landers, California earthquake, *Bull. Seism. Soc. Am.*, **84**, 668-691.
- Wald, D. J., Heaton, T. H., and Hudnut, K. W. (1996). The slip history of the 1994 Northridge, California, earthquake determined from strong-motion, teleseismic, GPS, and levelling data, *Bull. Seism. Soc. Amer.*, **86**, S49-S70.
- Ward, S., and Barrientos, S. (1986). An inversion for slip distribution and fault shape from geodetic observations of the 1983, Borah Peak, Idaho, earthquake, *J. Geophys. Res.*, **91**, 4909-19.
- Williams, C. R., Arnadottir, T., and Segall, P. (1993). Coseismic deformation and dislocation models of the 1989 Loma Prieta earthquake derived from Global Positioning System measurements, *J. Geophys. Res.*, **98**, 4567-4578.
- Williams, S., Bock, Y., and Fang, P. (1998). Integrated satellite interferometry: Tropospheric noise, GPS estimates, and implications for interferometric synthetic aperture radar products, *J. Geophys. Res.*, **103**, 27,051-27,068.
- Wolf, M., and Wingham, D. (1992). The status of the world's public-domain digital topography of the land and ice, *Geophys. Res. Lett.*, **19**, 2325-2328.
- Wright, T. J., Parsons, B. E., Jackson, J. A., Haynes, M., Fielding, E. J., England, P. C., and Clarke, P. J. (1999). Source parameters of the 1 October 1995 Dinar (Turkey) earthquake from SAR interferometry and seismic bodywave modelling, *Earth Plan. Sci. Lett.*, **172**, 23-27.
- Wyatt, F. K. (1988). Measurements of coseismic deformation in southern California: 1972-1982, *J. Geophys. Res.*, **93**, 7923-7942.
- Wyatt, F. K., Agnew, D. C., and Gladwin, M. (1994). Continuous measurements of crustal deformation for the 1992 Landers earthquake sequence, *Bull. Seism. Soc. Amer.*, **84**, 768-779.
- Zebker, H., and Goldstein, R. (1986). Topographic mapping from interferometric SAR observations, *J. Geophys. Res.*, **91**, 4993-5001.
- Zebker, H. A., Rosen, P. A., Goldstein, R. M., Gabriel, A., and Werner, C. L. (1994). On the derivation of coseismic displacement fields using differential radar interferometry: the Landers earthquake, *J. Geophys. Res.*, **99**, 19,617-19,634.
- Zebker, H. A., Rosen, P. A., and Hensley, S. (1997). Atmospheric effects in interferometric synthetic aperture radar surface deformation and topographic maps, *J. Geophys. Res.*, **102**, 7547-7563.
- Zumberge, J. F., Urban, M. P., Liu, R., and Neilan, R. E. (1996). International GPS Service 1995 Annual report, IGS Central Bureau, Pasadena.